Stress corrosion cracking, and corrosion fatigue in aluminium alloy 7017 with and without residual stresses

Thesis

UNRESTRICTED

STRESS CORROSION CRACKING AND CORROSION FATIGUE IN ALUMINIUM ALLOY 7017 WITH AND WITHOUT RESIDUAL STRESSES

A thesis submitted for the degree of

MASTER OF PHILOSOPHY

by

REINHOLD HERMANN

Dept of Material Science
The Open University
Milton Keynes
Bucks

May 1985

Date of Submission: MAY 1985
Date of Award: 27.2.86

SUMMARY

This thesis presents recent work on the stress corrosion cracking of aluminium alloy 7017 with and without residual stresses, and some results on corrosion fatigue.

Chapter I contains a literature review of the stress-corrosion cracking (SCC) and corrosion fatigue (CF) cracking mechanisms. It explains techniques, practices and the conclusions reached when Al-Zn-Mg-(Cu) are employed in such tests. The latter part of the review is devoted to recent work in aluminium alloys containing residual stresses when subjected to cyclic loading.

In Chapter II a description is given of the properties of the alloy, followed by specimen design, environmental aspects of testing, tensile loading of specimens and the deliberate introduction of residual stresses to test pieces for both stress corrosion and corrosion fatigue studies.

Chapter III outlines the experimental results of SCC without residual stress. Here the kinetics of sub-critical crack growth are assessed by analysing the v-K curves of the alloy when stress-corroded in various moist air environments. The effects of pre-exposure to salt solution prior to loading is described in the light of these experiments.

Also in Chapter III corrosion behaviour is discussed where specimens are deliberately pre-loaded in compression prior to SCC testing. It is shown that crack growth can be achieved without bolt-loading. The effects of environment and morphology of fractures are described and compared with those of Chapter III.

Chapter IV examines the corrosion fatigue behaviour of the alloy under the influence of residual stresses and cyclic loading, with reference to crack growth rates under compressive loading, frequency and pre-exposure effects. A model for assessing the residual stress ahead of the crack tip is suggested, using data from crack closure measurements.

ACKNOWLEDGEMENTS

I would like to thank Professor C W N Newey, Head of the Materials Science Discipline of the Open University, for the provision of laboratory facilities, and Professor C N Reid, my supervisor, for his continuous and active interest in the work.

Thanks are also extended to Dr G M Scamans and Dr N J H Holroyd of Alcan International Limited, Banbury, for providing the alloy for this study, for the use of certain facilities in the project, and for discussion and advice freely given.

Finally I would like to thank my wife, Avril, for the typing of the thesis and for her encouragement.

Aims and Objectives of This Study

This project was conceived as a result of an accidental discovery. During a study of torsional fatigue in a hollow extrusion of the aluminium alloy 6082 (or HE 30) containing circular holes, a specimen was accidentally overloaded and it was found that fatigue cracks initiated and grew radially from the holes in new locations that had been strained compressively by the overload. The effect was attributed to the development of tensile residual stresses at the sites of crack initiation. It is generally accepted that a tensile stress is required to cause stress corrosion cracking (SCC). The question was raised whether overloads could give rise to stresses that result in stress corrosion cracking and corrosion fatigue (CF). If it is possible to grow a stress corrosion crack after subjecting the material to an overload, how does the resulting residual stress dictate crack length, crack velocity and morphology of cracking?

The aim of this study is to describe the effects of deliberate overloads on the incidence of SCC and the effects of frequency, mean load level and humidity on the rate of growth of corrosion fatigue in the medium strength aluminium alloy 7017.

CONTENTS

Chapter IV

CHAPTER I LITERATURE REVIEW

Metallurgical Aspects of Aluminium Alloy 7017

Although aluminium is a soft metal, high strength:weight ratios can be achieved by certain alloying elements because most aluminium alloys respond to age or precipitation hardening. This brief review represents the basic principles of this phenomenon which applies generally to the 7000 series aluminium alloys containing zinc and magnesium.

A requirement to enable age hardening of an alloy to be obtained is that there should be a decrease in the solid solubility of one or more alloying elements as the temperature decreases. This is exploited in the following steps of the heat treatment:

1) During solution treatment at high temperature (eg 465° C) the alloying elements are dissolved in the aluminium matrix.

2) Once dissolved the alloy is quenched by rapidly cooling to room temperature to obtain a supersaturated solid solution of the alloying elements in the aluminium matrix. This operation is very effectively done by plunging the hot alloy into cold water, but the thermal contractioninvolved introduces into the alloy internal residual stresses which tend to be compressive at the surface and tensile at the core.

These stresses are associated with dimensional instability, particularly when stresses approach levels near the yield stress of the material. For example, quenching may cause buckling of thin plates. It is normal practice to overcome such residual quenching stresses by stretching the alloy to beyond yield after quenching, but frequently cooling rates are controlled to minimise the levels of residual stress. The extent to which slower quenching rates can be tolerated is governed by what is known as quench sensitivity. During slow cooling there is a tendency for some solute elements to precipitate out as coarse particles which will reduce the level of supersaturation and the response of the alloy to age hardening. In order to strike a compromise between these ill-effects of high and low quench rates, most high strength aluminium alloys are quenched into a fused salt bath at 180° C and held for a certain time before cooling to room temperature.

3) Age hardening is the final stage of the heat treatment and is used to develop the mechanical properties required in the heat treated alloy. The solid solution has to be decomposed to form fine precipitates and this is achieved by ageing the alloy at two different temperatures.

In 7000 series alloys, the precipitation sequence can be represented as follows: solid solution → spherical GP zone → ordered GP zones → η' (or M', semicoherent hexagonal $MgZn_2$) → η (or M, coherent hexagonal $MgZn_2$) + T phase (probably hexagonal Mg_{32} $[Al\ Zn]_{49}$).

In these alloys Guinier-Preston (GP) zones are ordered, spherical clusters, rich in Zn and Mg, which retain the structure of the aluminium-rich f.c.c. matrix and remain coherent with it. In some alloys (eg Al-Cu) the zones are platelets which may only be one or two atom planes in thickness. The planes on which these zones are formed is (100). The intermediate precipitate, the semicoherent phase may nucleate at sites of GP-zones.

The first ageing treatment is carried out at room temperature to refine the GP-zones, while the second is performed between 90-150° C, usually in two stages, one at 121° C for 24 hours and the other at 171° C for 4-6 hours. The first stage grows the GP-zones and the higher ageing temperature is mainly responsible for the nucleation of the η' phase. This two stage ageing treatment results in a significant increase in resistance to stress corrosion cracking with only little loss of tensile properties.

The phases η' and η are frequently present in grain boundaries, especially after slow cooling from the solution-heat-treatment temperature, but grain boundary precipitates can also form during ageing.

When precipitation occurs in the alloy, a zone near the grain boundary is found to be depleted of precipitates. This precipitate-free zone (PFZ) is formed due to the diffusion of solute atoms into the boundary where subsequently precipitates of different particle sizes are formed. Three types are noted: the biggest type is produced by the S-phase (Al-Cu-Mg-phase) or Cu Mg Al_2 and is about 10-30μm in diameter; the intermediate type is bigger than 1μm and is basically made up of inclusions or coarse constituents; the small type of precipitates have diameters of .1μm and are made up from intermetallic compounds as dispersoids containing the elements chromium manganese and zirconium.

Possibly the most important addition to the Al-Zn-Mg-Cu alloys besides Mg and Zn are Cr, Mn and Zr. Small amounts in these elements to the 7000 series Al-alloy raises the recrystallisation temperatures and changes the grain shape from an equiaxed to an elongated shape with irregular boundaries. By forming small particles they have the

capability to pin grain boundaries, thereby retarding recrystallisation and partially preserving the elongated grain shape formed during rolling of the plate. The difficulty in propagating SCC cracks perpendicular to the elongated grains is primarily responsible for the improved SCC performance in the longitudinal and transverse directions of alloys of the 7000 series containing chromium, manganese and zirconium.

The additions of up to 1% of copper do not change the basic precipitation mechanism and its strengthening effect is only modest, but it increases the resistance to SCC quite considerably, although higher increases cause severe problems during welding. Small amounts of iron and silicon are also present in the alloy as tramp elements. Although these elements have little effect on the SCC resistance, their presence is a primary factor in the determination of the fracture toughness. High amounts of Fe and Si lower K_{IC} and alloys containing these elements show an increasing quench sensitivity. Thus, decreasing Fe and Si contents help minimise quench sensitivity and also increases the fracture toughness (1,2).

A fine balance therefore exists between the amounts of alloying elements and age hardening to give the alloy its strength, toughness, resistance to SCC and weldability.

Modes of Sub-Critical Crack Growth in Aluminium Alloys

High strength aluminium alloys today are of great importance to our technological society. Some of the best known applications are in the aerospace industry, involving the construction of rockets, aircraft and spacecraft, but most applications are to be found 'on the ground' in truck frames, high strength cryogenic weldments, sheet metal work, hydraulic pipes, heavy duty welded structures in pipelines, cladding plates on armoured vehicles, forgings of various kinds and a great number of load-bearing structures.

In service high strength aluminium alloys occasionally fail at stresses far below the yield strength due to stress corrosion cracking (SCC) or corrosion fatigue (CF), phenomena which occur under certain environmental conditions.

The main purpose of this investigation is to present some quantitative SCC and CF data for the alloy 7017 and to review critically the importance of these results. Stress corrosion cracking is defined as environment-assisted crack growth occurring under static tensile stress, applied either externally or as part of an internal residual stress. Corrosion fatigue is defined as environment-assisted crack growth occurring under a cyclically varying tensile stress. Appropriately, linear elastic fracture mechanics (LEFM) analysis will be used, since the stress intensity factor K provides a good description of the stress intensity near a crack tip under the relative low stresses which are usually involved in SCC and CF.

Although SCC and CF of most high strength aluminium alloys have been studied in detail, very little is known or reported in the literature in respect of the alloy 7017, and it is fair to say that the very complex phenomena of SCC and CF are still far from being clearly understood.

SCC of Aluminium and its Alloys

Pure aluminium has been shown not to be susceptible to SCC, and as with most other f.c.c. metals it is tolerant to hydrogen embrittlement (3) but additions of impurities frequently form sites where a catalytic reaction can promote failure when subjected to certain environments (4,5).

The presence of an aqueous environment promotes galvanic effects causing corrosion currents to flow and thereby generating hydrogen that may be absorbed in the alloy.

For hydrogen to enter the metal it requires penetration through the oxide layer, and it has been shown (6) that Al_2O_3 is a very effective barrier to atomic hydrogen. It is thought that entry is made possible by irregularities or mechanical disruption in the oxide film creating an easy path for entry, also causing enhanced corrosion and dissociation of the environmental medium which produces more hydrogen at the surface. Adsorbtion and diffusion can occur subsequently. Other mechanisms of hydrogen formation at the metal oxide interface have been described (7) where the oxide film is not disrupted. The higher mobility of protons and electrons enables them to penetrate the oxide and a possible mechanism of hydrogen formation at the metal/oxide interface was proposed.

In spite of the passivity of the Al_2O_3 layer it is shown that certain conditions (eg. in the presence of halide ions, Cu^{2+} and Fe^{3+} ions) an attack by the corrosion medium on the oxide film is possible (4). Localised cells of corrosion are formed, promoting and encouraging hydrogen evolution and disruption of the oxide film. This action is further enhanced by the presence of impurities and precipitated alloying elements making it possible to break the oxide barrier, also producing a number of oxidation products which further increases corrosion. This is often associated with production of more atomic hydrogen creating an easy path for adsorbtion and diffusion.

Once protection by the oxide film is lost, the disruption by specific ions no longer plays a significant role and dissolution of the metal occurs. It has been reported (3) that the amphoteric layer Al_2O_3 is unstable when the pH of the solution is outside the range from 5.5 to 8.5. Localised anodic dissolution (LAD) has been described by many workers in the SCC field eg.(9,10,11)and a number of models have been proposed in which the dissolution processes are followed by hydrolysis with the reduction of the local pH to 3 - 3.5 at the crack tip. Many researchers regard this as the necessary condition for the initiation of hydrogen embrittlement (HE). SCC is regarded as a two-pronged attack on the alloy by mechanical and (electro-) chemical means and as a result it is not always possible to isolate the operating mechanism of LAD and HE although the origin of atomic hydrogen need not be the stress corrosion reaction. For instance,

hydrogen may be provided by reaction of the alloy with a humid air atmosphere and the water vapour may be ionised by suitable potentials (13). These conditions discourage anodic dissolution, in fact LAD must be ruled out in the absence of condensation.

Kinetic observations offer much better evidence against the LAD mechanism (14), although they do not completely rule out the possibility that LAD controls crack growth; it was shown that the rate of corrosion product removal from the crack tip of a growing crack is determined by the ratio of the crack opening to the thickness of metal dissolved at the grain boundaries (15). When this ratio is high the rate of metal removal should not be limiting the crack growth rate, according to LAD. The majority of kinetic studies have used experimental data of SCC in aluminium alloys which were interpreted in terms of LAD, because electrochemical and crack growth rate data allowed them to do so (15). Many researchers question the use of electrochemical polarisation against crack growth rate data in identifying the controlling mechanism of SCC on the basis that in anodic polarisation the electrolyte in the crack becomes more acidic, so that both mechanisms LAD and hydrogen release including HE are accelerated (38. 45,35).

There are a number of good models and experimental data which support HE to be controlling SCC in aluminium alloys (3). Thin alloy foil hydrogen permeability studies under anodic and cathodic polarisation and discontinuous SCC crack growth are in support of the HE hypothesis. Though crack growth was delayed by cathodic polarisation, it was indeed accelerated by anodic polarisation with the conclusion the HE is the controlling SCC mechanism, taking discontinuous crack growth to be evidence for HE.
In the same study (3) it was shown that hydrogen is known to reduce ductility by making cross slip more difficult. Other studies and evidence by transmission electron micrographs (16) showed that hydrogen bubbles were associated with cracks in aluminium alloys, in particular with precipitates forming sites for the accumulation of hydrogen at points in the metal. Therefore stresses around hydrogen bubbles are sometimes thought to be the culprit for HE but work done by other researchers (16) proposed that for some cases dissolved atomic hydrogen is transformed to the molecular form under the influence by the electron beam of the microscope and this suggests that it is decohesion by hydrogen that causes embrittlement rather than stresses induced by bubbles of high pressure H_2 gas. This was indeed confirmed in a separate study (17).

Studies of the fracture surfaces of the alloy 7075 using Auger electron spectroscopy showed that the intergranular nature of SCC was the result of magnesium segregation at grain boundaries and this suggested the possibility that MgH may be formed during SCC and that HE may be caused by the fracture of hydrides (18).

These researchers showed that when the ratio between Mg:Zn is reduced, together with additions of Mn, Zr, Cr and Ti, the grains become finer and the resistance of the alloy to SCC improves. Subsequently, a kinetic study on the oxide layer of Al - 5.5 Zn - 2.5 Mg was performed in humid air with the results that Mg - concentrations at grain boundaries diffused to the oxide layer with the formation of MgO. The grain boundary became eventually enriched in aluminium but the concentration of Mg at grain boundaries was high enough to form both species MgH and MgH_2 which reduced the alloy's plasticity in 95% relative humidity without condensation of water taking place (19).

Workers using strain rate data to reveal SCC behaviour of aluminium alloy showed some interesting observations using varying strain rates in dry and humid air (20). At high rates of straining (10^{-2} - 10^{-4} s^{-1}) the mechanical properties showed no dependence on various ageing treatments and the fracture was ductile. At low strain rate (10^{-4} - 10^{-6} 5^{-1}) for samples aged in humid air, losses of up to 60% of plasticity were found and the resulting fracture surfaces became intergranularly embrittled.

Because aluminium alloys are most widely used in air, gaseous environments are of particular interest. In the past tests have shown that the water vapour content in many gaseous environments has an important effect on SCC in many aluminium alloys (23); furthermore, when the moisture of the environment is removed the alloys do not appear to embrittle, that is, tensile strength and ductility are not reduced. The same is true when the same alloys are charged with high purity H_2 gas at ambient temperature; for instance the alloys 6061-T6, 7075-T73 and 7039-T61 do notsuffer any change in mechanical properties as indicated above (24,25). It has been shown that SCC of various aluminium alloys in most gases is caused by the content of water vapour rather than the individual carrier gas (26). It is not clear however, if the mechanism of cracking is by hydrogen adsorbtion or localised dissolution of the ruptured film or a combination of the two. An attempt was made(27) to characterise the range of adsorbtion to facilitate cracking, in a study of Al-Zn-Mg single

crystals. It was found that ductile fractures were observed for specimens tested in dry air, hydrogen and argon, but brittle fractures were found on specimens tested in liquid metal, aqueous solutions and moist air. It was suggested that environmentally assisted cracking was accomplished by localised slip due to high localised strains, involving adsorbtion of hydrogen which facilitates the nucleation of dislocations at the crack tip. If this occurs hydrogen can be transported by dislocation to sites where it becomes innocuous or forms voids ahead of the crack tip (28). However, it is thought that for a macroscopic embrittlement a critical localised concentration of hydrogen is needed to favour slip distribution. Other sites can be grain boundaries, precipitates or dispersoids and it has been shown that the presence of hydrogen can damage grain boundaries in particular in those alloys where Mg is precipitated from the matrix (26, 35). In this case an intergranular fracture is produced.

In some papers reviewed so far it has been accepted that a tensile stress is necessary for SCC, and this was obtained by applying an external load. However, tensile residual stresses can also be induced at the tip of a notch by compressive pre-loading. In a study (33) it was shown that SCC can nucleate and grow in a variety of moist air environments without external loading. Recent experiments on compressively pre-loaded compact tension specimens made of medium carbon steel have shown that stage II fatigue crack can nucleate and grow under cyclic compressive loads, provided the specimens contain a sufficient level of residual stress (34).

Corrosion Fatigue of Aluminium Alloys

When considering the susceptibility of aluminium alloys to fatigue the question arises of whether SCC and CF are combined or separate entities. A general model has been proposed (36) that describes the mechanical, metallurgical and environmental components of corrosion fatigue, in which the crack growth rate in CF is regarded as being the sum of that occuring by fatigue in an inert environment and the crack velocity due to stress corrosion. This description was also proposed later by Speidel (37). Unfortunately this appears to be an incomplete description of CF in this class of alloy (7000-series) as pointed out by Holroyd et al (38). It was argued that the application of a super-position model is not valid when the velocity of SCC is very different from that by fatigue in an inert environment even when the stage II plateau velocity in SCC is

applicable to the fatigue loading cycle. Furthermore, there is no reason why inert atmosphere fatigue should be an additive rather than a competitive process and an attempt was made to describe the mechanism which controls the transition between SCC and CF. Fatigue crack propagation tests were carried out in different environments on 7075-T6 and 2024-T3 alloys by Vogelsang and Schijve (39) and it was shown that the transition from tensile to shear failure is suppressed by aggresive environments, but is promoted by an inert environment.

SCC and CF in the Presence of Residual Stress

The effects of tensile overloads on the incubation time in SCC and fatigue have been investigated by Hanish et al (40). They concluded that tensile overloads of pre-cracked 7075-T651 alloy resulted in significantly increased incubation times for stress corrosion cracking. The incubation time increased with the overload but the effects were larger at lower stress intensities for given increments of overload. The incubation retardation effects, they concluded, were due to residual compressive stresses introduced at the crack tip by stress overloads.

While all previously mentioned work considered CF and SCC under tensile loading, fatigue tests on round bar specimens carried out by Gerber and Fuchs (41) on the same alloy as used by Hanish et al (40) showed that when specimens were cycled with a compressive mean stress, non-propagating cracks are produced. They measured and compared the experimental crack depth with the theoretical one, using the Tresca Yield Criterion, showing that good agreement existed by comparing both results. The notch depth was estimated by using a slip-line field solution for stresses within the yield zone, and its modification for the yield zone, with the assumption that the yield criterion is the same in tension and compression.

They concluded that fatigue crack growth depends on a critical tensile stress perpendicular to the direction of the propagation in the vicinity of the crack tip, and the depth to which a non-propagating crack will grow is related to the stress distribution in the test piece during cyclic loading.

Using photoelastic techniques, an investigation was made by Hubbard (42) of fatigue crack growth in centrally notched specimens of the same alloy as the two previous investigators which were also subjected to cyclic

compressive loading. A fracture mechanics model relating crack growth to residual stress at the root of the notch was proposed and it was concluded that for a particular crack length and maximum compressive load the tensile residual stress field is slightly smaller than the plastic zone, however the residual strain field is not significantly changed as the crack grows through it. In contrast to this conclusion, Saal (43) carried fatigue crack growth tests with compressive mean load using centrally notched specimens and found that the residual stress field in the vicinity of the notch is released as the fatigue crack is growing, and ceases as the crack reaches the plastic zone boundary. Crack propagation beyond the plastic zone depends on the stress intensity of the tensile load if the minimum load is compressive.

More recent work on compressively pre-loaded specimens of medium carbon steel have shown that stage II fatigue cracks can nucleate and grow under cyclic compressive loads provided the specimens contain a sufficient level of residual stress (34).

In order to study the effects of such stresses, notched specimens of the commercial alloy 7017-T651 have been loaded in compression. This gives rise to a residual tensile stress ahead of the notch tip after the load has been removed. The fatigue crack growth in the presence of such residual stresses was described in an abridged presentation presented at a recent conference (44).

Residual stresses may be introduced in an earlier stage of material production, quenching after solution treatment being a good example. Rapid cooling sets up steep gradients of temperature and thermal contraction to reduce the difference in contraction between neighbouring locations some non-uniform plastic strain occurs leading to tensile residual stresses at the centre, and compressive stresses at the surface (21). Residual stresses are also caused during SCC, that is after initiation of a crack. It has been reported that corrosion products in a running crack can raise the stress intensity at the tip to higher levels by a process called product wedging (22). Under both sources of stress, SCC failure is influenced by the shape and orientation of the grains, the applied stress and by metallurgical parameters.

Summary of Literature Review

In this review of the literature two important aspects of SCC and CF have been discussed: firstly, the proposed mechanisms of SCC in aluminium alloys and secondly the importance of overload effects on SCC and CF of the alloy 7017.

The review has shown that the mechanism of cracking in aluminium alloys can be either by the model of localised anodic dissolution (LAD) or by hydrogen embrittlement. In the early 1960's, aluminium alloys in aqueous solutions were generally accepted to fail intergranularly by LAD but later it was shown quite convincingly that embrittlement by hydrogen could occur in moist air without dissolution taking place. However, no critical experiments have yet been carried out to prove conclusively that HE is taking place in environments where LAD is thought to be the mechanism of cracking. The possibility should not be excluded that in metal/liquid environments LAD is required for HE to occur, especially when the LAD process is followed by hydrolysis, creating conditions for a continuous supply of hydrogen.

With regard to the review on overload effects, there was a sparsity of publications on fatigue in overloaded aluminium alloys in general (41, 42, 43). In three papers the alloy 7075 was used in the investigations, and in most cases the specimens were cyclically loaded in tension after the application of an 'overload' to the material. In the case of SCC, reference 38 described the effect of overloads on the incubation time for cracking of 7075, and with the exception of reference 33, no other publications have been cited where the stress corrosion cracking was initiated and propagated after a compressive overload. Therefore the objective of this study to investigate the effect of compressive overload on both SCC and CF of the alloy 7017 is justified.

CHAPTER II EXPERIMENTAL DETAILS

In this section the mechanical and environmental details of the experiments are described so that they need not be repeated in the description of experimental results.

1 a) Properties and Chemical Composition of 7017

Properties and composition of the alloy are given in Table 1. It is shown that 7017 is an Al-Mg-Zn-Cu alloy specifically designed for high strength to be used as weldable armour plate. The American Aluminium Association classify aluminium alloysunder a numbering system in which the 7xxx denotes the series containing zinc. In addition to 5% Zn the alloy also contains 2.5%Mg and other fractional percentages of Fe, Si, Mn and Cu. The optimum hardened condition is denoted by T651 and is obtained by the following treatment:

hot rolled
solution treatment at 465° C followed by
cold water quench
stretched by 2½%
aged for 48 h at room temperature for refinement of the GP zones
aged at 90° C for 8 h and 150° C for 8 h.

The tensile strength and fracture toughness of the heat treated alloy are also given in Table 1.

b) Grain Shape, Size and Orientation

SCC failure of most aluminium alloys is intergranular, so grain size, shape and orientation have a pronounced effect on the performance of the alloys in a given environment. 7017 is no exception and a typical microstructure is presented in Figure 1 together with an indication of the rolling plane and direction. Micrographs of the alloy reveal an elongated, fibrous microstructure, which is typical for all cold rolled aluminium alloys.

2 Specimen Design

Two specimen designs are used in the study, namely

i) Double-Cantilever-Beam (DCB) specimens which are used in the experiments reported in chapters III and IV, and

ii) Compact Tension Specimens (CTS) used in the fatigue tests reported in chapter V.

The shape and dimensions of the DCB specimens are shown in Figure 2a. Dimensions are as follows: length (L) 98 mm, height (2h) 30 mm and thickness (B) 25.4mm. They are machined from a 400 x 200 x 30 mm^3 plate with their long axes parallel to the rolling direction of the plate and with notches cut parallel to the rolling plane (ie. with the notch plane lying perpendicular to the short transverse direction) so that cracks would run in the rolling plane without branching or deviation. Figure 3 shows the rolling direction and orientation of the plate. 'Fixed displacement loading' was achieved by turning a pair of hardened steel bolts threaded into the machined notch of the specimen until a particular deflection is reached or until a crack is introduced by 'pop-in.'

CTS were produced in exactly the same way as described for DCB specimens. Because of limited thickness of the plate a full size CTS could not be made from this material, so a substandard size was used.

The geometry is given in Figure 2b and the dimensions are: length (L) 25 mm, height (2H) 25 mm and thickness (B) 10 mm. In both designs the final side surface preparation was by mechanical polishing employing paraffin as lubricant. The final finish was via a 1/4 μm diamond paste followed by degreasing with acetone and finally analar methanol.

3 Environmental Aspects

Quantitive experimental data, such as crack initiation, crack growth rate and threshold stress intensity values, are sensitive to the environment used in SCC. It is worthwhile specifying them appropriately. Two moist air environments have been used in this study:

i) 95% relative humidity (RH), this is produced in a humidity cabinet by keeping a distilled water bath at a constant temperature of 40° C. This environment is easily maintained over long periods of time.

ii) Ordinary laboratory environment at room temperature produced humidity levels between 52 and 58% RH.

In some experiments these environments have been used in conjunction with pre-exposure. Some test pieces have been pre-soaked for 15 or 30 days in a 3% NaCl solution at room temperature before being subjected to the above environments.

4 External Loading of DCB specimens

The use of DCB specimens offers several advantages over other methods such as simple design, its self-stressing capability, low manufacturing cost and ease in generating useful data (29, 30). By observing the position of the crack tip as a function of time, measurements are made of the crack velocity V as a function of the crack length a. Under loading to a fixed displacement μ, the plane strain stress intensity K_I depends on the crack length according to the expression

$$K_I = \frac{\mu Eh}{4} \frac{[3h\,(a + 0.6h)^2 + h^3]^{\frac{1}{2}}}{[(a + 0.6h)^3 + h^2 a]} \qquad (1)$$

where μ is the deflection between the two arms of the specimen at the load line, E is Young's Modulus, a is the crack length measured from the load line and h is the half height of the specimen.

Using this expression, the observed variation of V with a can be interpreted as a relation between V and K_I. Under fixed displacement a crack grows at a decreasing rate until $V \rightarrow 0$ as K_I approaches a threshold value (K_{ISCC}). DCB specimens were used to find K_{ISCC} and the V-K curve.

In practice, the loading bolts are turned until a crack is produced by 'pop-in' at the notch tip. By increasing the displacement this crack can be made to grow rapidly. The fracture toughness K_{IC} is found from Equation 1 by measuring the deflection μ and the crack length at which rapid crack extension occurs. This process is repeated several times giving a number of K_{IC} values. The bolts are then fixed to give a constant crack opening displacement and the specimen is then subjected to the environment. At the onset of cracking the load at the bolts and the stress intensity K_I at the crack tip decrease as the crack length

increases. The slope of the resulting crack length versus time curve gives the crack growth rate and allows this to be correlated with the value of K_I. With a fixed displacement and progressively increasing crack length K_I decreases until it reaches a value below which the crack growth ceases. This K-level is the threshold value K_{ISCC} for the prevailing experimental and environmental conditions. Schematically the events of SCC are illustrated in Figure 4.

Measurements of crack length were carried out daily after cracks had been initiated, using an optical microscope capable of measuring to a resolution of ±0.02 mm. The crack lengths on both sides were measured. The measuring intervals after 500 h were twice weekly, and after 1,000 h once weekly. After breaking the specimen open the fracture surfaces were thoroughly examined in an optical microscope. Internal crack length measurements were taken and finally the morphology was examined in a Scanning Electron Microscope (SEM).

5 Introduction of Residual Stresses in DCB Specimens by Pre-loading in Compression

It is accepted that a tensile residual stress is necessary inorder to get SCC and in most work reported this has been obtained by applying an external load. However, tensile residual stresses can be induced into a specimen by compressive pre-loading. Compressive pre-loading causes plastic deformation at the notch tip and on unloading this region develops a residual tensile stress field.

In these experiments DCB specimens (see Figure 2a) have been used and in order to arrive at a reasonable compressive pre-load for this specimen geometry, it is worth estimating the force required for general yielding of the material. The equation is given below (46):

$$G_y = \sigma_y B t \left(1 - \frac{2c}{t}\right) \qquad (2)$$

where σ_y is the proof stress (441 MNm^{-2}), B is the thickness of the specimen (25.4 mm), t is the height of the specimen (30 mm) and c is the distance of the neutral axis from the notch tip (0.41t).
The force required for general yielding was calculated to be 64.5 kN.

A series of specimens is pre-loaded compressively in an Instron servo-

hydraulic testing machine (model 8031) to a maximum load between -20 and -45 kN After unloading the specimens were transferred to various environments. Incremental crack length measurements were made at 10 minute intervals in the first hour and every hour between 2 and 8 hours. Subsequent measurements were recorded daily and above 1000 h, weekly. The remaining experimental procedure is identical with the bolt-loaded specimens.

6 Corrosion Fatigue in the Presence of Tensile Residual Stress. Specimen preparation, pre-loading and fatigue data

Specimens were machined as described under 2. The geometry was 25 x 25 x 10 mm^3 (see Figure 2b) and, consistent with the SCC specimens, a sharp V-notch was cut parallel to the rolling plane. A 120Ω strain gauge was affixed to the back face which was used to measure the change in strain as a function of crack length, and to detect crack closure when an increasing compressive load was applied at the end of the fatigue test. To one side surface a small measuring scale (produced onto film from a microscope graticule) was stuck, which was used to measure accurately the fatigue crack length. The accuracy was about ± 0.01 mm.

Specimens were now pre-loaded compressively in a servohydraulic Instron testing machine (model 8031) to -6 kN, -8 kN and -10 kN. Ramp speed was -.05 kN/second and the load was held at these levels for 30 seconds. After unloading they were cyclicaly loaded in laboratory air, using an Instron 8031 machine operating under load control. These events are shown schematically in Figure 17. Mean load levels and amplitudes were selected so that the net loads on the specimens remained always compressive. The mean load levels were in the range of -0.5 kN to -1.5 kN and a constant amplitude of 0.5 kN was used throughout. A sinusoidal waveform was used with two frequencies, namely 5 and 25 Hz.

Pre-loading in compression causes a plastic zone to form at the notch tip. On unloading a tensile residual stress is developed in this region which is bi-axial at the surface and tri-axial in the interior. In order to demonstrate this a specimen was pre-loaded to a known compressive load and while still under load, a brittle lacquer was sprayed onto the surface and allowed to dry. The load was now slowly removed causing the lacquer to crack. The result is shown in Figure 18 revealing a residual tensile stress surrounding the notch tip. It can be seen that the centre of

concentric rings lies a small distance ahead of the notch tip.

When the fatigue crack had ceased growing, a tensile load was applied to break the specimen open and the fracture surfaces were examined in a SEM. Further crack length measurements were carried out to compare crack lengths at different points on the surface and the mode of cracking was determined.

Relative humidity (RH) levels were recorded on a Forster Cambridge Clear-span M501. All fatigue work was carried out in laboratory air with humidities between 50 - 60% RH.

TABLE 1 CHEMICAL COMPOSITION IN WT%

OF 7017-T651 AND SHORT TRANSVERSE

MECHANICAL PROPERTIES

Cu	Mn	Mg	Fe	Si	Zn	Ti	Cr	Zr	Al
.11	.29	2.30	.35	.18	4.78	.04	.15	.14	Balance

	.2% PS	UTS	%EL	E	K_{IC}
	441 MPa	488	12	71 GNm^{-2}	26 $MNm^{-3/2}$

CHAPTER III

Stress Corrosion Cracking of 7017 in Moist Air (Under Applied Stresses)

1 Under Applied Stresses

SCC experiments on bolt-loaded DCB specimens have been carried out. Crack growth data were obtained as a function of plane strain stress intensity and the effects on initiation and crack velocity of pre-exposure of the alloy to 3% NaCl solution were explored. It is shown that crack growth rates are enhanced by more than a factor of 2 by pre-exposure when other parameters are kept constant, and that in moist air the alloy does not recover from the effect of pre-exposure.

For all experiments described here it is found that the K_I independent region of the V-K curve (where V is the crack velocity and K is the stress intensity) the plateau velocity is sensitive to the combination of environment and pre-exposure treatment. Also, it appears that the threshold value of K is not unique to the alloy but is affected by the pre-exposure and the environment. Crack morphology shows that SCC is predominantly intergranular after a sharp crack is produced initially by pop-in.

1.1 Experimental Results and Discussion

Effects of Environmental Conditions

Tests were carried out on DCB specimens under constant displacement loading. Graphs of crack length versus time are illustrated in Figure 5 for each of two invironments (95 and 55% RH), with pre-exposure for 15 and 30 days in the 3% NaCl solution and without pre-exposure.

The Firgue shows that after some small delay (SCC initiation time, the time from loading to the first onset of SCC) crack growth was rapid for the first 500 h in the 95% RH environment, slowing down at 750 h, and almost stopping after 1250 h. The other two curves illustrate the results when the specimens had the same initial K_I value but were subjected to laboratory air at 55% RH. The initiation times were longer before the first crack growth was observed, but the shapes of these two curves are similar to that of the 95% environment. Crack growth rates are determined from these plots by measuring the slopes of tangents, and the

resulting crack velocity is now plotted against the calculated stress intensity. This is illustrated in Figure 6 showing the effect of stress intensity on the stress corrosion cracking velocity. All four curves exhibit plateaus (Region II) but at different velocities, where the velocity is independent of the stress intensity, followed by a 'knee', where the crack velocity decreases with falling stress intensity (Region I). The slope, when measured on a single specimen, is found to be finite at least to velocities of 10^{-10} to 11^{-11} ms^{-1}, and this suggests that no true K_{ISCC} exists and that the apparent value of K_{ISCC} depends very much on the patience of the researcher.

Speidel and Hyatt (28) proposed that the K_{ISCC} is defined as the stress intensity at which the crack velocity reaches a value of 10^{-10} ms^{-1} (the lowest that can be measured in a 30 day test). This definition of K_{ISCC} has been used throughout this work. Measurements over 1500 h or 75 days show that the value of K_{ISCC} for the two environments (95% RH and 55% RH) are found to be 5.5 and 9.6 and for the pre-exposed specimens 4.8 and 7.8 $MNm^{-3/2}$ respectively. Three important findings are evident from these tests so far:

i) the environment has a marked effect on initiation and on the SCC velocity in Region II,

ii) the apparent thresholdvalue of K_I is different in the two environments,

iii) pre-exposure lowers the K_{ISCC} in a given environment.

To explore further the effect of pre-exposure, one specimen was pre-exposed to salt-solution but then allowed to 'incubate' for 30 days in laboratory air. A second testpiece was pre-exposed for 30 days in salt solution. The idea behind this approach was firstly to demonstrate whether the alloy would recover from the effect of pre-exposure and secondly whether a longer pre-exposure further reduces the time of initiation and changes the character of the v-K curve to a higher plateau velocity. Specimens were prepared as described earlier, bolt-loaded after pre-exposure to K-values approximately equal to those in the previous experiment and subjected to the same environment (95% RH) as discussed. The results are shown in Figures 7 and 8 showing curves of time versus crack extension and crack velocity versus stress intensity respectively. Overall, the results are very similar to the cases discussed

previously. After little delay crack growth is rapid at first and the velocities are approximately equal to those in Figures 5 and 6. The specimen left in laboratory air after pre-exposure shows no recovery and indeed the plateau velocity is marginally higher compared with the results in Figure 6. Pre-exposure under these conditions is irreversible. The values of K_{ISCC} are not affected although the 'knee' im both V-K curves is moved to smaller K_I values. All experimental data are summarised in Table 2. Extending pre-exposure from 15 to 30 days did not enhance the extent of rate of cracking.

As to the nature of the irreversible effect of pre-exposure, it is suggested that the initiation of pitting of the alloy in chloride solution proceeds in four discreet steps: i) the adsorption of the chloride on the alloy's oxide film, ii) the chemical reaction of the anion with the Al in the oxide lattice, producing at least one stable hydroxy-chloride, iii) the thinning of the oxide film by dissolution and iv) the direct attack of the exposed alloy by the aggressive chloride anions. This will result in a number of complexes which eventually undergo hydrolysis. Localised anodic dissolution (LAD) reactions can produce hydrogen ions which may be adsorbed at pitting sites either within the aluminium or possibly along a network of grain boundaries beneath the surface of the alloy. LAD and hydrogen adsorption will eventually be stopped when a hydrogen equilibrium profile is set up. On the application of stress to the crack tip and exposure to moist air environment, additional hydrogen is made abailable from the reaction of the water vapour with the aluminium alloy. It is assumed that this additional hydrogen is also absorbed into the alloy, resulting eventually in loss of ductility, embrittlement and SCC by intergranular failure. For this reason the additional amount of hydrogen made available by pre-exposure in salt solution is responsible for higher crack velocities and the increase in the plateaus as shown in Figures 6 and 8. It may also be responsible for the decrease in the thrshold value of K_{ISCC}.

The presence of water in the environment was found to be necessary to cause SCC. No crack growth was observed when a pre-exposed specimen was loaded and held for 500 h in dry air, but cracking was initiated when the same specimen was transferred to the 95% RH environment. All experiments have been performed in duplicates and some in triplicate and experimental data are summarised in Table 2.

1.2 Crack Morphology

When all crack growth ceased specimens were broken open and optically examined. The dry air test showed no crack extension after 500 h other than the pre-crack and this was confirmed when the fracture was carefully examined in the SEM.

Figure 9a shows the fracture surfaces in the two environments, both with and without pre-exposure. It shows that specimens A and C, B and D have comparable crack length, but a considerable amount of fibrous grain lifting is noticed on the fractures surfaces of A and C. This is probably due to the crack tunnelling which took place during SCC. All crack fronts are curved convexly with respect to the notch. The fracture surfaces of specimens E and F are much smoother showing very little crack tunnelling.

Examination in the SEM revealed that all SCC surfaces are intergranularly embrittled. There is no difference between the morphology of cracks grown in Region II and Region I (see Figures 9b and c). However, when Region I cracks were examined at high magnification, it was found that in some areas a number of small striations were visible. The 'crack arrest markings' are shown in Figure 10; the crack propagation direction is as indicated by the arrow. They occasionally extend from one grain to the next and this seems to be evidence for discontinuous crack propagation. Similar observations have been made in the past on this alloy and 7018 (31) and on a high purity Al-Zn-Mg-alloy (32), although in this case the arrest marking were of transgranular nature.

1.3 Summary to Section 1

SCC experiments on DCB specimens have been carried out, and the following has been established:-

a) The initiation time depends on the environment; it increases as the RH is reduced. Pre-exposure in salt solution prior to bolt loading shortens the initiation time and increases the initial crack velocity.

b) The crack propagation rate at a fiven value of K_I is also environment dependent. The rates are faster in the more moist environment.

c) The Region II crack velocity depends on the environment.

d) The alloy shows no recovery from pre-exposure to a salt solution after storage in dry air.

e) K_{ISCC}, the threshold stress intensity, is environment-dependent; the more moist environment shows the smaller apparent K_{ISCC} value after 1500 h.

f) Crack morphologies examined in the SEM show that the fractures are intergranular but in areas where the operating velocity is strongly stress dependent 'arrest markings' are found.

TABLE 2 SUMMARY OF SCC DATA FROM TESTS

Test No	Environment	Initial K_I $MNm^{-3/2}$	Initiation time h	Plateau crack velocity ms^{-1}	App. K_{ISCC} $MNm^{-3/2}$	Total crack length at side surface mm	Total time of test h
A	55% RH	22.6	216	2.5×10^{-9}	9.2	19	2750
B	95% RH	21.5	16	1.04×10^{-8}	5.6	30.5	3000
		22.6	18	9.5×10^{-9}	5.2	36	3000
C	Pre-exp +55% RH	22.9	48	$4.5 - 5.2 \times 10^{-9}$	7.7	26.25	4600
D	Pre-exp + 95% RH	20.9	>12 <24	3×10^{-8}	5.1	34	2400
E	Pre-exp 15 days in NaCl + 30 days lab air +95% RH	21.4	>16	2.85×10^{-8}	4.8	38	1900
F	Pre-exp 30 days in NaCl + 95% RH	21.5	16	3.80×10^{-8}	5.4	35	1900

2 Under Residual Stresses

Stress corrosion cracking experiments have been carried out on double-cantilever-beam specimens. The specimens were first subjected to a known compressive load which caused plastic deformation at the notch tip. On unloading, this region developed a residual tensile stress field and on subsequent exposure to moist air at 40% C (95% RH) and in laboratory air at 22° C (55% RH) intergranular cracks formed. These cracks grew at a decelerating rate until they stopped. The final crack length increased with the value of the initial compressive pre-load, provided this was below the value for general yielding of the alloy. The effect of pre-exposure of the alloy to salt solution is examined. Electron Fractography has been used to correlate changes in surface morphology with crack growth rate.

2.1 Experimental Results and Discussion

Effect of Pre-Load on Crack Growth

In all tests shown here most crack growth occurs in the first 200 h of exposure. Cracks then decelerate until arrest occurs. After 2000 h the crack length on the surface is different from that at the centre of the same specimen. In the environment A (95% RH) for pre-loads up to -30 kN the crack length measured at the surface is only half that measured at the centre (Fig 11a). The specimens pre-loaded above -30 kN showed an increase in the final crack length at the surface because the tensile residual stress increased with compressive pre-load. It was also observed that rapid crack initiation and extension by ductile tearing occurred during the initial unloading at the beginning of the test. This ductile tearing increased as the compressive pre-load increased regardless of the environment used. This general observation concerning crack extension by ductile tearing is consistent with the results of environment B, when specimens were subjected to laboratory air environment of approximately 55% RH. The dependence of the final crack length on compressive pre-load and environment is shown in Figure 11 a-d. The initial crack growth has been

calculated by drawing crack length versus time curves, Figure 12 a-d, and measuring the slope of the tangent of each curve. The velocities given in Table 3 seem to suggest that there is a trend of increasing initial crack velocity with increased compressive pre-load by roughly one order of magnitude in environment A, while in B there is a twofold increase with increasing pre-load. Comparing the initial crack velocities with the Region II velocities it appears that there is a similarity, except for specimens pre-loaded to -45 KN, where there is a twofold increase between initial velocity and plateau velocity.

2.2 Effects of Environment

Crack initiation time and the initial propagation rate are shown to be dependent on the magnitude of the pre-load, and hence the residual stress. Comparing the results for environments A and B at constant residual stress, the initiation time is reduced by increasing the relative humidity, showing that the concentration of water vapour has a strong influence over crack initiation. An environmental effect is also found in tests C and D, where the specimens were pre-soaked in salt solution prior to compressive pre-loading. Comparing the values of initiation time for identical pre-load and environments (95% RH, Table 3 and Figure 12 a+c) it can be seen that pre-exposure reduces the initiation time, the biggest effect occurring in specimens pre-loaded to -25 kN. The effect of RH is also seen in tests B and D (both are pre-exposed), Figure 12 b and d; the extent of pre-exposure is seen on all pre-loads and in every case the initiation time is found to be smaller in the pre-exposed alloys. Crack velocities are about equal for the same environments and pre-exposure, but different between 95% RH and 55% RH for the same pre-load. An increase of crack velocity with RH has been observed on bolt loaded specimens, when the plateau velocity of the V-K curve was raised to higher levels by the change in environment (see Figures 6 and 7).

All experimental data are summarised in Table 3.

2.3 Crack Morphology

Four photographs are shown in Figure 13 representing a view of the fracture appearance after the specimens were broken open. Generally, for pre-loads ranging from -30 kN and above, ductile tearing occured from the notch tip during unloading, thereby nucleating a crack which

subsequently grew by SCC. Within a few minutes of unloading a crack formed along a line of inclusions, suggesting that ductile tearing took place at the interface between precipitates or inclusions and the metal matrix. This is shown in Figure 14. Note the heavily distorted surface around the notch and slip bands that lie at approximately 45° to the crack.

All six specimens tested in environment A show an increase in crack length with increasing pre-load, Figure 13 a. The first three show a convex crack front with respect to the notch, while the next three are clearly concave, with some reversed bowing towards the edges of the specimen. For specimens pre-loaded above -30 kN three distinct morphologies are visible: the grey fracture just above the notch "a" has the same fracture appearance as the 'break open' fracture at the top of region "c". Between these two similar areas lies the light region of SCC, region "b". More detail is given in Figure 15, which is a magnified view of the fracture surface of the specimen pre-loaded to -45 kN.

This observation is consistent for the fracture appearance in Figure 13 b the fractures of test environment B (55% RH). However, the fractures of environments C and D shown in Figure 13 c and d appear to have larger amounts of reversed bowing, in particular the specimen pre-loaded to -42 kN, although the amount of ductile tearing on these specimens is approximately the same.

Fractographic examination in the SEM confirmed that the fracture appearance next to the notch for specimens pre-loaded at -30 kN and above is identical to the 'break open' fracture. The SCC fracture surface of one of the specimens (-30 kN pre-load) shown in Figure 16a is predominantly intergranular at high magnification, and a number of steps or 'terraces' are visible at lower magnification, formed when the crack front was climbing from one 'pancake' grain to another, Figure 16b. In these areas secondary cracks are observed, growing into the plane of the specimen.

The morphology of fractures produced by the 55% RH environment showed identical features when examined in the SEM. Additionally, in areas near the 'break open' fracture the surface showed a number of 'arrest markings' similar to those observed in the bolt-loaded specimens. However, when a comparison is made between the morphologies of fractures from specimens pre-exposed to salt solution and unexposed, it is found that differences exist on the ductile tearing fractures. This is shown in Figure 16 c - e

for the unexposed, f-h for the pre-exposed alloy. Figure 16c shows the area close to the notch (unexposed alloy), where tearing produced a number of small transgranular facets of regular size, and these appear generally uniform. Note the change in morphology in Figure 16f for the pre-exposed area near the notch tip. The large regular facets and very small ductile dimples are replaced by smaller facets with a 'brittle' appearance: some have distinctly flat fracture surfaces. Note particularly the change in fracture between the end of ductile tearing and the beginning of the SCC fracture, Figures 16d and g. Again the ductile facets appear smooth and regular in Figure 16d, whereas in 16 g the morphology of the transgranular area is 'rugged' and less uniform. The smoothness has disappeared. Similar comments can be made when comparing the two fractures of Figures 16e and 16h. Once more the un-exposed alloy shows a very smooth and regular ductile pull-out. Note a number of arrest markings at the end of the SCC fracture which lie perpendicular to the crack propagation direction (CPD) indicated by the arrow. These crack arrest markings are found with frequent regularity on both SCC fracture surfaces.

This comparison suggests that pre-exposure of the alloy prior to pre-loading has an effect on the fracture morphology during crack initiation. Although the main fracture surface appears ductile transgranular, pockets of inter-granular areas are found near the notch, more frequently in the pre-exposed alloy. The change in dimple size for the pre-exposed alloy is observed generally.

Mechanistically these stress corrosion results suggest that after hydrogen has entered the alloy, the compressive pre-load changes the mechanical behaviour of the alloy in such a way that ductility is impared when the compressive load is removed, resulting in a semi-brittle fracture. Therefore the degree and change in ductility depends on the local availability of hydrogen and the tri-axial stress state in the crack tip region.

3 Summary of Section 2

Compressively pre-loaded V-notch specimens of 7017-T651 alloy show stress corrosion cracking in 95% RH, 55% RH and also when pre-exposed to salt solution and subjected to the two moist environments. The crack grow at a decelerating rate and finally stop. The final crack length increased with the value of the initial pre-load, but did not depend on the potency of the environments. Although for a given pre-load the final crack lengths are approximately the same (the residual stress is the same), crack initiation time and crack velocities are environment dependent. The effect of pre-exposure of the alloy to salt solution reduces the initiation time and increases the crack velocity. The observation is consistent with results on bolt-loaded specimens.

Fractography indicates:

a) that SCC is predominantly intergranular,

b) that at compressive pre-load of -30 kN and above there occurs some ductile rupture during and after the release of the pre-load and

c) that some of the ductile failure is environment assisted.

4 Summary of Chapter III

In this part of the study, two different approaches have been used and it is concluded that under an applied stress, stress corrosion cracking can occur in this alloy, the kinetics of which are denoted by the shape and appearance of the V-K curve. It was further shown that the effect of pre-exposure prior to applying stress changed the plateau velocity to higher velocities and this effect was found to depend on the pre-exposure time. It was concluded that hydrogen already in the alloy prior to crack initiation was responsible for this behaviour.

The section on SCC under residual stress showed that cracks can be initiated from the root of the notch. The initial crack velocity was shown to be equal to the plateau velocity and the effect of pre-exposure was found to be similar to that found under applied stresses. The morphology of fracture suggested that cracks grew in both cases in an intergranular fashion and the conclusion to be drawn from this evidence is that the mechanism of embrittlement appears to be the same. No conclusion can be drawn from these results on whether pre-exposure had an effect on the residual stress field produced during pre-loading although some fractographic evidence suggests a possible effect of pre-exposure on the ductility of the alloy.

TABLE 3 SUMMARY OF SCC DATA FROM PRE-COMPRESSION TESTS

Test No	Environment	Compressive pre-load kN	Inititation time, h	Final crack length, mm, after 2000 h			Initial velocity da/dt, ms^{-1}
				at the surface	at the centre	SCC at centre	
A	95% RH at 40° C	-20	288	.53	1.07	1.07	2.3×10^{-10}
		-25	165	.90/.91*	1.86	1.86	2.3×10^{-9}
		-30	3	1.45	2.31	2.31	5.2×10^{-9}
		-35	1	1.71/1.94*	2.99	2.48	7.7×10^{-9}
		-40	30 min	2.96	3.35	2.23	1.9×10^{-8}
		-45	10 min	3.73/3.88*	3.31	2.01	2.8×10^{-8}
B	55% RH in lab air at RT	-25	800	1.08/1.12*	1.98	1.98	3.5×10^{-9}
		-35	175 (22)	2.13/2.16*	2.80	2.15	6.5×10^{-9}
		-45	5	3.12/3.91*	3.45	2.28	7.4×10^{-9}
C	Pre-exposed to salt solution +95% RH at 40° C			1000h/2000h			
		-25	22	1.20/1.32	2.18	2.18	6.3×10^{-9}
		-35	<2	2.44/2.67	3.06	2.09	1.2×10^{-8}
		-42	15 min	4.12/4.18	3.63	2.57	1.73×10^{-8}
D	Pre exposed to salt solution +55% RH in lab air at RT	-25	126	1.21/1.36	2.10	2.10	4.03×10^{-9}
		-35	72 (6)	1.92/2.54	2.70	1.72	4.6×10^{-9}
		-42	10 min	2.79/3.70	4.10	3.08	8.2×10^{-9}

Figures with * indicate measured at 5000 h

CHAPTER IV

Corrosion Fatigue Behaviour in Moist Air of the Alloy 7017 Containing Residual Stresses

1 Introduction

Corrosion fatigue (CF) experiments have been carried out on miniature compact tension specimens. Firstly the specimens were subjected to a deliberate compressive pre-load and after unloading fatigue cracks were grown under cyclic compressive stresses. The effects of the residual stress, frequency and environment on the fatigue crack growth and mode of cracking have been assessed in the light of the following experimental results and observations.

2 Experimental results and discussion

a) Effect of pre-load and mean load on fatigue crack growth

After pre-loading and loading cyclically in compression, a fatigue crack was detected at the notch tip after a certain number of load cycles ('incubation cycles'). The initial crack growth rate was largest and the growth rate subsequently fell gradually to zero. Table 4 gives a summary of all tests carried out in lab air environment. It shows the total crack length for various values of pre-load (residual stress), mean load level and frequency.

At first glance it can be seen that the final crack length for a given pre-load and mean load is independent of frequency. Furthermore, the final crack length increases with mean load level and is largest at - 0.5 kN. The same trend is evident at all three pre-loads. The results at 25 Hz are plotted in Figures 19a, b and c, showing graphs of crack length against number of cycles. Figures 20a, b and c are plots for a frequency of 5 Hz. Although the trends are the same as those for 25 Hz, there is a major difference with regard to the onset of fatigue crack propagation. The number of 'incubation cycles' is very much greater but the final crack length has the same value as that measured at 25 Hz. In each case it can be seen that the final crack length increased with the value of the initial pre-load (residual stress).

The dependence of the final crack length on the pre-load is readily understood. Crack growth will cease when the stress intensity range at

the crack tip, ΔK, falls to a threshold value for the material ΔK_{th}. ΔK depends on the tensile stress range which in turn depends on the sum of the (static, tensile) residual stress σ_r and the (cyclic compressive) applied stress σ_a. The crack stops at a place somewhere near the boundary of the plastic zone, where the value of σ_r has fallen to a small, critical value. Therefore the final crack length increases with the plastic zone size (ie. increases with the pre-load).

By examining Figure 21 it can be seen that for a given pre-load the final crack length increases with mean load level. This arises because the place at which the superimposed tensile stress range ($\sigma_r + \sigma_a$) falls to the critical value, gets further from the notch as the mean load level increases. A constant amplitude (0.5 kN) was used throughout but this was not fully effective in causing fatigue because only the tensile stress range controls fatigue crack growth. Some of the load amplitude was therefore "wasted" in certain tests because the crack was closed during parts of the load cycle (see Table 4 for those cases where the minimum load is less than the closure load). The effect of an increase in mean load is to increase the effective (crack opening) part of the load cycle.

The initial crack velocity $(da/dN)_o$ has been estimated by measuring the slope of the tangent to the a/N curve at small values of a, and these values $(da/dN)_o$ appear in Table 5.

There is a tendency for the initial crack velocity $(da/dN)_o$ to increase with the value of pre-load from - 6 to - 10 kN at constant mean level. According to the Paris-Erdogan relation:

$$da/dN = C(\Delta K)^m \qquad (3)$$

the rate of crack growth da/dN depends on the tensile stress intensity range ΔK and these results would suggest that an increase in $(da/dN)_o$ reflects an increase in ΔK_o, the stress intensity range near the notch tip. In order to investigate this effect the constant C and m have been determined for this alloy by tension-tension fatigue in the same specimen design. The results are shown in Figure 22, in which log da/dN is plotted against log ΔK; the constant C is the intercept of the growth data when the extrapolated line reached $\Delta K = 1$ $MNm^{-3/2}$ and the exponent m is the slope of this curve.

With these two constants known it is now possible to calculate the stress intensity range ΔK_o using the observed crack growth rate from Table 5; results are given in Table 6. The apparent increase in ΔK_o with pre-load for a given cyclic load is small for a mean load of - 0.5 kN but becomes more pronounced using the mean load levels of - 1.0 and - 1.5 kN.

From crack closure measurements it is possible to calculate the theoretical value of $(da/dN)_o$. The closure load values are determined from a compliance graph when backface strain is plotted against compressive pre-load before fatigue and after, when cracks have ceased growing. Graphically this is shown in Figure 23. To express the stress intensity at the notch tip the effective fatigue load range is determined from

$$F_{eff} = F_{max} - F_{cl} \qquad (4)$$

where F_{max} is the maximum applied load (see Figure 17) and F_{cl} is the measured closure load (see Figure 23). The stress intensity near the notch tip is calculated by the use of the K calibration equation in which P is replaced by F_{eff}

$$K_I = \frac{Y \times F_{eff}}{B\, W^{\frac{1}{2}}} \qquad (5)$$

where $Y = f(a) = 8.10$, W is the length from the loading line to the back of the specimen and B is the specimen thickness (see Figure 2).

The results of the theoretical value of da/dN and the stress intensity is given in Table 7 and it is apparent that with increasing pre-load both the ΔK_I and the velocity seem to increase. In most cases, the predicted values of $(da/dN)_{th}$ compare reasonably well with the observed values (see Table 5). The discrepancies that do exist are thought to arise partly from the accuracy of the method by which the crack closure data are determined. Furthermore the observed initial growth rates $(da/dN)_o$ are measured from the initial slopes of Figures 19 and 20 and it is difficult to locate the tangents accurately at the beginning of the curves, so the observed growth rates are also prone to some error.

b) Effect of pre-exposure on crack initiation and crack growth

It was shown by results in Chapters 3 and 4 that pre-exposure of the alloy to aqueous salt solution had a drastic effect on initiation and crack propagation velocity and in view of these results fatigue tests were carried

out to assess the behaviour of the alloy when pre-exposed to salt solution for several days. This was followed by compressive pre-loading and cyclic loading.

Figure 24 (a, b) shows two plots of crack lengths versus N (number of cycles) at 25 Hz and 5 Hz for two different exposure times, 7 and 15 days. For the alloys fatigued at 25 Hz it can be seen that the crack initiation 'times' differ by 1500 cycles; the specimen pre-soaked for 15 days failed first with an initial crack velocity $(da/dN)_o = 9.2 \times 10^{-8} ms^{-1}$. The other curve has a similar shape but is displaced. The number of cycles to crack initiation is increased but the final crack length is approximately the same. The initial crack velocity when measured from the tangent of the a - t curve appears slightly lower, $(7.3 \times 10^{-8} ms^{-1})$ when compared with the velocity of the 15 days pre-soaked test. The effect of changed frequency is shown in Figure 24b when the pre-exposed specimens were fatigued at a frequency of 5 Hz. The crack initiation period and the initial crack velocity da/dN are almost identical for both pre-exposures; the two curves overlap during the first 10,000 load cycles. The number of cycles required to initiate a crack is found to be independent of frequency when pre-exposed to salt solution in marked contrast to the results of Figures 19 and 20 for alloy that had not been pre-exposed. It is suggested that there is some environmental interaction with the alloy in the crack tip region to account for the delay in crack initiation at 5 Hz. The initial crack growth rates $(da/dN)_o$ seem to be the same for pre-exposed or unexposed alloy. The numerical results from pre-exposure tests are summarised in Table 8.

c) Estimation of residual stresses using the back-face strain gauge method

Back-face strain (BFS) measurements have so far been used to assess the range of the stress intensity ΔK at the notch tip by crack closure measurements.

Another use of BFS is to estimate the unknown residual stress distribution created by pre-loading of the CT specimen. By cyclic loading, a fatigue crack will grow slowly from the notch tip through the region of residual stress. When the crack grows by a small increment the tensile residual stress over that increment is relaxed, and this unbalances the remaining residual stress ahead of the crack tip. To restore the balance it is assumed that the uncracked section of the specimen undergoes pure linear bending which is detected by the BFS gauge.

Residual stress originally present at a point a distance t from back-face is

$$\sigma''_R(t) = E\left[\frac{tg(t)}{2} - 3t\int_t^T \frac{g(x)}{x}\,dx + \int_t^T g(x)dx\right] \qquad (6)$$

where E is Young's Modulus, and g(x) is the strain gradient. The derivation of this equation is given in the appendix on page 46.

For one specimen pre-loaded to -8 kN, fatigues with a mean load level of -0.5 kN and a frequency of 25 Hz, the residual stress originally present is shown in Figure 27. This is obtained by measuring the back-face strain after compressive pre-loading and at intervals of crack growth, with the cyclic fatigue load removed from the specimen. This procedure is repeated for several increases in crack length until crack growth ceases. Figure 27 shows both the change in strain levels and the distribution of the residual stress until crack growth ceases. The strain curve becomes almost a straight line.

By describing the model of assessment of residual stresses in CT specimens (47) it is assumed that the specimen undergoes pure linear bending across the unbroken ligament. This assumption is wrong in some details. However as a 'first-order approximation' it is considered to be useful. No doubt the absolute figures in Figure 27 would be different if finite element analysis was applied to the problem, but the values plotted are of plausible magnitudes, and do not exceed the yield stress of the alloy (488 MNm^{-2}).

d) Fatigue Crack Morphologies

i) Effects of frequency on mode of cracking

For tests carried out at a frequency of 25 Hz fractures shown in Figure 28 and observed in the SEM revleal a transgranular fracture mode for the initial stages of growth followed by a mixture of flat-transgranular and intergranular cracking. This is shown in Figure 29 a-d. In picture a) the overall specimen morphology is shown at low magnification. The area near the notch tip in b) reveals that the crack was initiated by a 'ductile' failure, similar to that shown in Chapter III. The dimples appear large bu then occurs a change into some 'flat' mode which is transgranular; occasionally ridges, steps or terraces are found, see Figure 29 c-d, although in this last micrograph there is also intergranular cracking. This is an area which is from the 'knee' of the curve in Figure 19a (-10 kN pre-load, mean load -0.5 kN ± 0.5 kN).

The fracture mode for tests carried at a frequency of 5 Hz is found to be similar in all respects except the area such as shown in Figure 29d. On all specimens fatigued at 5 Hz it was found that the amount of intergranular fracture had increased in comparison to the corresponding specimens tested at 25 Hz and the amount of transgranular fracture decreased. Measurements of the total crack length indicated that for a constant pre-load (residual stress) the transgranular crack length increased as the mean load level became less compressive and the intergranular crack length was almost independent of mean load level at both frequencies. The graphs of Figures 19 and 20: crack length v number of cycles have the same shape (for a given mean load and amplitude) at 25 Hz and 5 Hz but (as discussed above) at 25 Hz crack growth begins after a short delay of a few thousand cycles, whereas at 5 Hz the delay is several thousand cycles longer. It appears that there is a critical 'incubation time' for the onset of intergranular cracking. When the frequency is high the 'incubation time' is insufficient to allow a critical amount of the CF medium (Hydrogen) to be accumulated. Therefore the main fracture mode is transgranular. When the frequency is low (5 Hz) sufficient time is given, and it is for this reason why larger areas of intergranular cracking mode are observed. Once more this is found to be independent of mean load levels.

ii) Effects of pre-exposure on the mode of cracking

Specimens pre-exposed for 7 and 15 days showed that fatigue crack initiation is delayed by several thousand cycles when fatigued at 25 Hz (see Figures 19b and 24a). From this point of view it may be suggested that pre-exposure is advantageous because crack initiation is delayed. However the cracking morphologies on these pre-exposed specimens show that initiation is by a ductile type of failure followed by some larger areas of 'flat' trans- and eventually intergranular cracking. The whole fracture surface looks like a typical intergranular SCC fracture and much less than the fracture of Figures 28 and 29. As a comparison Figures 30 a, b and 31 a, b show the fracture appearance of the pre-exposed specimens.

Although there is no clearly defined zone between the change in fracture mode from flat transgranular to intergranular, the amount of intergranular fracture for both frequencies and pre-exposure times is larger than for specimens without pre-exposure treatment. The initial crack growth rates are lower in all pre-exposed tests, independent of frequency, and this suggest the the crack growth rate depends on the mode of cracking.

All cracks that are observed to grow at slower velocity rates show larger amounts of intergranular fracture.

This is in contrast to the observations and results in both Chapters III and IV, where it was shown that pre-exposure made no difference to the fracture appearance although the plateau velocity was increased by a factor of between 2 - 4; in these experiments all fractures were predominantly intergranular. Noticeable on all fatigue fractures is the absence of fatigue striations (striations indicate that the crack is advancing by small, clearly visible steps). This is thought to be due to the compressive parts of the loading cycle which flattens the striations. It explains why the transgranular fracture appears predominantly 'flat'. However, there is one exception to this observation: at a frequency of 25 Hz and a mean load level of ±0.5 kN striations are seen but only on certain planes where the two fracture surfaces do not 'rub' together (see Figure 32). Once the crack front leaves this plane the striations are again 'damaged' and the 'flat' transgranular fracture is observed.
The change to an intergranular fracture occurs late in each individual test, suggesting that the interaction between the environment and the crack tip is dependent on the level of the embrittling species (hydrogen) ahead of the crack tip.

3 Summary to this chapter

1 A region of tensile residual stress has been formed at the notch tip by pre-loading in compression.

2 Fatigue cracks have been formed at the notch tip by subsequent cyclic loading in compression; after a number of load cycles a crack nucleated and grew at a diminishing rate (da/dN) until it stopped.

3 The final crack length increased with increases in

i) the pre-load

ii) the mean load

(for a given amplitude). It was independent of the loading frequency.

4 The cycles required for crack initiation were found to be dependent on the frequency; initiation at 5 Hz required ten times as many

cycles as that for 25 Hz. Pre-exposure of the alloy to salt solution at 5 Hz had little effect on initiation, but it delayed initiation by several thousand cycles at 25 Hz.

5 The mode of cracking is frequency dependent; at 5 Hz larger areas of intergranular cracking are observed whereas at 25 Hz the fracture surfaces are predominantly transgranular with little intergranular fracture.

6 When pre-exposed to salt solution the amount of intergranular cracking caused by given cyclic loading is larger than that without pre-exposure.

7 A first order theoretical model is suggested to estimate the residual stresses using the back-face strain gauge method. It is assumed that the specimen undergoes pure linear bending, and values appear of plausible magnitude since the yield stress of the alloy is not exceeded.

4 Summary of Discussion

In order to appreciate fully the results in this part of the study it is important to identify the controlling factor in compression fatigue. It is proposed that this is the tensile stress intensity range, ΔK_I in Equation 3. The range of stress intensity arises from the sum of the (static, tensile) residual stress σ_R and the (cyclic, compressive) applied stress σ_a. As σ_R increases, the tensile stress intensity range increases and this was clearly shown to be the case when the compressive pre-load was increased. For a given value of σ_R the range of ΔK can be reduced by making the applied stress σ_a more negative (compressive), either by reducing the mean load level or the amplitude or both. In this case, not all the variation in applied load is effective in causing fatigue because the crack is not fully open during parts of the load cycle. This effect of mean stress and amplitude was observed in practice. It can therefore be concluded that even under compressive cyclic loading, the fatigue crack growth is still controlled by the tensile stress intensity range ΔK (Summary 2 & 3).

In summary 5 & 6 it was noted that the proportion of intergranular fracture increased as the frequency and pre-exposure prior to pre-loading was changed. This result may be explained by a possible interaction between the alloy and moist air in the crack tip region during fatigue. By reducing the frequency from 25 to 5 Hz, the number of cycles required to initiate a crack increased but the author is unable to offer a convincing argument or a model to explain this phenomenon. It is proposed that, during the crack initiation period, there occurs the build-up of a critical amount of embrittling species in the crack tip region. It is also proposed that in the case of PE in salt-solution, the crack morphology was changed by hydrogen introduced to the alloy during the pre-exposure treatment. However, a critical level of hydrogen is achieved only when an interaction with moist air is possible.

A lesson to be learned from the application of compressive overloading is that such loading could result in the premature failure of components which, without overloading, would withstand the effects of environments and stress. It is therefore asked whether 'shake-down' procedures on pressure vessels are sometimes detrimental to the lifetime of the component. The resulting plastic deformation occuring in the vicinity of flaws or cracks may be sufficient to form fields of tensile residual stresses and under certain environmental conditions cracks may develop to critical dimensions.

Overall Conclusion

This study has confirmed that cracking of the alloy 7017 can take place during static and cyclic loading, and that the kinetics of such cracking is affected by pre-exposure to corrosive environments. A tensile residual stress field was set up by compressively pre-loading the alloy and this was shown to give rise to SCC failure in moist air, and it is suggested that this occurred by a mechanism of hydrogen embrittlement. Similarly, compressive cyclic loading showed that fatigue cracks can nucleate and grow from a notch preloaded in compression. These are original observations, not previously reported. Back-face-strain measurements have been used to provide data from which the residual stresses at the tip of the notch have been estimated, and it was concluded that results were satisfactory as a first order model. Finally, it may be pointed out that the overall objective of this research study was met and the major aims achieved.

TABLE 4

SUMMARY OF FINAL CRACK LENGTHS (IN MM) AND CLOSURE LOADS (IN kN, SHOWN IN BRACKETS) AS A FUNCTION OF MEAN LOAD LEVEL, PRE-LOAD AND FREQUENCY

FATIGUE MEAN LEVEL	-1.5 kN ± 0.5 kN			-1 kN ± 0.5 kN			-0.5 kN ± 0.5 kN		
FREQUENCY	5 Hz	10 Hz	25 Hz	5 Hz	10 Hz	25 Hz	5 Hz	10 Hz	25 Hz
PRE-LOAD									
-10 kN	1.30	1.17	1.27 (-2.05)	1.70	1.60	1.60 (-2.25)	2.35	2.31	2.30 (-2.25)
-8 kN	0.67	0.74	0.63 (-1.20)	0.88	0.98	0.85 (-1.75)	1.37	1.24	1.40 (-1.90)
-6 kN	0.28	0.22	0.30	0.55	0.42	0.52 (-1.15)	0.71	0.65	0.70 (-1.40)

TABLE 5

INITIAL CRACK VELOCITY da /dN WITH CHANGING MEAN LOAD LEVEL, PRE-LOAD AND FREQUENCY

FATIGUE MEAN LEVEL/kN	-1.5 ± 0.5		-1.0 ± 0.5		-0.5 ± -.5	
FREQUENCY/Hz	5	25	5	25	5	25
PRE-LOAD/kN						
-10	8.3×10^{-8}	1.1×10^{-7}	1.11×10^{-7}	1.25×10^{-7}	1.25×10^{-7}	1.3×10^{-7}
-8	5.2×10^{-8}	6.7×10^{-8}	1.0×10^{-7}	8.3×10^{-8}	1.2×10^{-7}	1.25×10^{-7}
-6	2.8×10^{-8}	2.1×10^{-8}	3.0×10^{-8}	4.8×10^{-8}	8.7×10^{-8}	7.2×10^{-8}

TABLE 6

STRESS INTENSITY AND PREDICTED CRACK VELOCITY FROM CRACK CLOSURE MEASUREMENT, f = 25 Hz

$$F_{eff} = F_{max} - F_{cl}, \quad K_I = \frac{y \times F_{eff}}{BW^{\frac{1}{2}}}, \quad da/dN = C(\Delta K)^m$$

$$y = f(a) = 8.10 \qquad = 1.1 \times 10^{-9} (\Delta K)^{2.66}$$

MEAN LOAD/kN	-1.5 ± 0.5			-1.0 ± 0.5			-.5 ± 0.5		
Pre-load/kN	(da/dN) th	F_{eff}	K_I	(da/dN) th	F_{eff}	K_I	(da/dN) th	F_{eff}	K_I
-10	1.3×10^{-7}	-1.05	6.02	5×10^{-7}	-1.75	10.00	9.8×10^{-7}	-2.25	12.9
-8	1.6×10^{-9}	-0.20	1.15	2×10^{-7}	-1.25	7.16	6.3×10^{-7}	-1.90	10.9
-6	-	-	-	3.6×10^{-8}	-0.65	3.72	2.8×10^{-7}	-1.40	8.01

TABLE 7

INITIAL STRESS INTENSITY RANGE ΔK_o USING CRACK VELOCITIES da/dN FROM TABLE 5

$$da/dN = C(\Delta K)^m$$

$$= 1.1 \times 10^{-9} (\Delta K)^{2.66}$$

FATIGUE MEAN LEVEL/kN	-1.5 ± 0.5		-1.0 ± 0.5		-0.5 ± -.5	
FREQUENCY/Hz	5	25	5	25	5	25
PRE-LOAD/kN						
-10	5.08	5.65	5.67	5.93	5.93	6.00
-8	4.26	4.68	5.45	5.08	5.84	5.92
-6	3.38	3.03	3.47	4.13	5.17	4.82

TABLE 8

SUMMARY OF FINAL CRACK LENGTH (IN MM), CRACK VELOCITY $(da/dN)_o$ AND EFFECTIVE CRACK CLOSURE LOAD (kN), f = 5 AND 25 Hz

COMPRESSIVE PRE-LOAD: -8 kN, MEAN LOAD: -0.5 kN

PRE-EXPOSED FOR 7 AND 15 DAYS PRIOR TO CYCLIC LOADING

Pre-exposed 7 days				Pre-exposed 15 days					
Frequency Hz	Final Crack Length	$(da/dN)_o$	$(\Delta K_I)_o$	Final Crack Length	$(da/dN)_o$	$(\Delta K_I)_o$	F_{eff}	$(da/dN)_{th}$	$(\Delta K_I)_{th}$
5	1.49	7.3×10^{-8}	4.84	1.31	8.3×10^{-8}	5.08	1.25	5.1×10^{-7}	10.05
25	1.42	7.2×10^{-8}	4.82	1.26	9.02×10^{-8}	5.24	1.85	5.3×10^{-7}	10.62

Appendix

Consider Figure 25 for the following derivations: (47)

i) Force Equilibrium

A force, F_1 in the y direction is lost by removal of a layer dx thick due to a crack growth increment

$F_1 = (\sigma_R dx)$ where σ_R is the residual stress in the layer.

This force must be replaced by a net force created by bending of the remaining section about an off-centre neutral axis; This introduces a net force F_2 in the y direction of

$$F_2 = -\tfrac{1}{2}\ \sigma'_R ft + \tfrac{1}{2}\ (\frac{1-f}{f})\ \sigma'_R\ (1-f)t$$

The terms on the right are the areas under the stress/distance graph.

$$F_2 = \frac{-t\ \sigma'_R}{2} \quad (\frac{2f-1}{f})$$

Equating forces F_1 and F_2:

$$\sigma_R = \frac{-t\ \sigma'_R}{2dx} \quad (2 - \frac{1}{f}) \ \ldots\ldots \qquad \text{(A1)}$$

There are two unknowns: σ_R and the fractional distance f of the neutral axis from the back face.

ii) Moment Equilibrium

To get f, take moments about O; the moment M_1 of the removed force ($\sigma_R dx\ (1-f)t$) must equal that associated with bending. The moment due to the bending deformation in a thin layer at position x is:

$$dM = \frac{x^2}{ft}\ \sigma'_R\ dx \quad \text{(where x is now measured from O).}$$

The total moment is obtained by summing the moments from all such layers:

$$M_2 = \frac{\sigma'_R}{ft} \int_t^T x^2\ dx$$

$$M_2 = \frac{\sigma'_R}{3ft}\ [\ (ft)^3 + (1-f)^3 t^3] = \frac{\sigma'_R t^2}{3f}\ [f^3 + (1-f)^3]$$

Equating the moments M_1 and M_2:

$$f = \frac{1}{3} \qquad \text{(A2)}$$

And putting into equation (6) σ_R is obtained

$$\sigma_R = \frac{\sigma'_R \, t}{2dx} \qquad \text{(A3)}$$

σ_R is the residual stress in the layer dx, situated a distance t from the back face of the specimen just prior to the crack extension. This is accompanied by a back face strain of ϵ', where $\sigma'_R = E\,\epsilon'$, with ϵ' as the strain measured by the strain gauge.

Now consider Figure 26 which depicts the effect of removing a layer dx at point 'x' on the stress at 't'.

Change of stress at x is

$$2Ed\,\epsilon'(x) \quad \left(\text{ie. } \frac{(1-f)}{f}\,\sigma'_R \text{ with } f = \frac{1}{3} \text{ and } \sigma'_R = Ed\,\epsilon'\right)$$

Change of stress at t is $[2Ed\,\epsilon'(x)]\,\dfrac{(t-\frac{x}{3})}{(\frac{2x}{3})} = Ed\,\epsilon'(x)\,(\frac{3t-x}{x})$

$$\text{or } d\sigma = Ed\,\epsilon'(x)\,(\frac{3t}{x} - 1)$$

Total change in stress at t due to removal of all layers between t and T:

$$\Delta\sigma = \int d\sigma = \int_t^T d\epsilon'(x)\,(\frac{3t}{x} - 1)$$

$$d\epsilon'(x) = (\frac{d\epsilon'}{dx})\,dx = g(x)\,dx$$

where g (x) is the rate of change of back face strain with changes in crack length.

$$\Delta\sigma = E\int_t^T [3t\,\frac{g(x)}{x} - g(x)\,dx \qquad \text{(A4)}$$

Combining equations (8) and (9) we get the <u>original</u> residual stress;

$$\sigma^{\#}_R = \sigma_R - \Delta\sigma$$

$$\sigma^{\#}_R(t) = \frac{Ed\,\epsilon'(t)t}{2dx} - \Delta\sigma(t)$$

Residual Stress originally present at a point a distance from back-face

$$\sigma''_R(t) = E\left[\frac{tg(t)}{2} - 3t\int_t^T \frac{g(x)}{x}\,dx + \int_t^T g(x)dx\right] \qquad (A5)$$

where E is Young's Modulus, and g(x) is the strain gradient.

FUTURE WORK

In order to gain better understanding of the mechanisms of environmental cracking, an extension of the work in Chapter III is in hand investigating the embrittlement in the 7000 series of aluminium alloys both in moist air and aqueous environment (NaCl). Of specific interest are pre-exposure tests on the behaviour of the plateau velocity of the V-K curve and the threshold values. Kinetic data on crack growth measurement offer the possibility of predicting the plateau velocities for a given pre-exposure time. Mechanistically such data could also help to explain grain boundary penetration theories of induced embrittlement due to the incubation period prior to crack initiation, in particular if there is a rate-controlling process involved.

In liquid environments the composition of the electrolyte at the crack tip can now be characterisedto assess the degree of chemical and electro-chemical activity in such areas. This has been made possible by quantifying species at the tip of the crack by two methods, Atomic Adsorption Spectroscopy (AA) and X-ray fluorences data (XRF). Other methods, such as the measurements of pH (micro pH paper) and potentials by a newly developed conducting bridge medium, allow such characterisation to be made specifically to small volume samples. The results so far suggest that there is a classical relationship between the concentration of Aluminium dissolved and the pH on the one hand, and the dependence of Aluminium concentration on chloride ion concentration. Mechanistically it will be possible to suggest a model demonstrating that in liquid environment the hydrogen embrittlement is initially triggered by dissolution at the tip of the crack. Dissolution at crack tips can be controlled by applying an external potential; anodically this would increase, and cathodically decrease the crack velocity. Of interest in this part of the future study is the relationship of both the Al and Cl ion concentration in the plateau region of the V-K curves.

A study of crack initiation and propagation using the shadow-optical method of Caustic shows promise in revealing the complex relationship in the crack tip region between the environment and the elastic behaviour, prior to and during crack propagation. This method allows a description of the elastic stress field in the vicinity of the crack tip without the knowledge of crack length, crack opening deflection or load. Results obtained so far show that the method is more than just a tool to determine stress intensity factors.

REFERENCES

(1) J W Martin, Precipitation Hardening, Pergamom Press Ltd, (1968)

(2) I J Polmear, Light Alloys - Metallurgy of Light Metals, Edward Arnold (Publishers) Ltd, (1981)

(3) R J Gest and A R Troiano, Corrosion 30, 8 pp 274-279 (1974

(4) H H Uhlig, Corrosion and Corrosion Control, John Wiley & Sons, New York, (1963)

(5) E H Dix, Journal Trans. Am. Institute Mining Met, Engrs., pp 1057-1127 (1950)

(6) C N Cochran, Journal of the Electrochemical Society, 108, 4, pp 317-321 (1961)

(7) J Draley and W Ruther, Corrosion 12, pp 441-448 (1956)

(8) G M Scamans, R Alani and P R Swann, Corrosion Science 16, 7, pp 443-459 (1976)

(9) A J Sedricks, J A S Green and D L Novak, 'Localised Corrosion', NACE - 3, p 569 (1974)

(10) B F Brown, C T Fujii and E P Dahlberg, Journal of Electrochem. Soc., 116, p 218 (1969)

(11) T H Nguyen, B F Brown and R T Foley, Corrosion 38, p 319 (1982)

(12) V A Marichev, Werkstoffe und Korrosion, 33, (1982) and 34, pp 300-308 (1983)

(13) G H Koch, Corrosion 35, 2 pp 73-78 (1979)

(14) R M Latanison, J C Turn, R C Compeau, Proceedings of Intern. Conf. in Mechanical Behaviour of Metals, Toronto, Canada, 2, p 475 (1979)

(15) H E Engell, The Theory of Stress Corrosion Cracking in Alloys, ed. J C Scully, p 86 (1971)

(16) G M Scamans, Journal of Materials Science, 13, pp 27-36 (1978)

(17) R Alani and P R Swann, British Corrosion Journal, 12, 2, pp 80-85 (1977)

(18) E C Pow, W W Gerberich and L E Toch, Scripta Met, 15, (1981)

(19) R K Viswanadham, T S Sun, and J A S Green, Corrosion 36, p 275 (1980)

(20) S W Ciaraldi, J L Nelson and E N Pugh, Effect of Hydrogen in Metals, ed. I M Bernstein, A W Thomson, Pittsburg, USA pp 438 (1981)

(21) E H Spuhler and C L Burton, Avoiding Stress Corrosion Cracking in High Strength Aluminium Alloy Structures, Alcoa Green Letter, Alcoa, August 1962

(22) D O Sprowls, Physical Metallurgy of Stress Corrosion Fracture ed. T N Rhodin, Interscience Publishers, New York, p 146 (1969)

(23) E H Dix, Acceleration of Rate of Corrosion by Constant Stresses, Trans. AIME 137, 11 (1940)

(24) J E Campbell, Effects of Hydrogen Gas on Metals at Ambient Temperature, DMIC Report S-31 (1970)

(25) R M Vennett and G S Ansell, A Study of Gaseous Hydrogen Damage in Certain FCC Metals, Trans. ASM 62, 1007 (1969)

(26) M O Speidel and M V Hyatt, Stress Corrosion Cracking of High Strength Aluminium Alloys, eds. M G Fontana and R W Staehle, Advances in Corrosion Science and Technology, Vol 2 (1972)

(27) S P Lynch, Corrosion Science, 22, 10 pp 925-937 (1982)

(28) J Albrecht, A W Thompson and I M Bernstein, Metallurgical Transaction A, Vol 10A, pp 1759-1766 (1979)

(29) M V Hyatt, Use of Pre-cracked Specimens in Stress Corrosion Testing of High Strength Aluminium Alloys, Corrosion 26 (1970)

(30) M O Speidel and M V Hyatt, in Advances in Corrosion Science and Technology, Vol 2, eds. M G Fontana and R W Staehle, Plenum Press, New York - London (1972)

(31) G M Scamans, Metallurgical Transactions A, Vol IIA, pp 846-850 (1980)

(32) J L Nelson and E N Pugh, Met. Trans. A, Vol 6A, pp 1459-60 (1975)

(33) R Hermann, Journal of Materials Science 16, pp 2381-86, Chapman & Hall (1980)

(34) C N Reid, K Williams and R Hermann, Fatigue of Engineering Materials and Structure, Vol 1, pp 267-270, Pergamon Press Oxford (1979)

(35) G M Scamans, N J H Holroyd, Alcan Internation Ltd, Banbury, Oxon, personal communication (1983)

(36.) J Shoju, H Takahashi, T Sueki and T Kondo, Transaction of ASME 103, pp 298-304 (1981)

(37) M O Speidel, ICAF Symposium, Lausanne, CH (1975)

(38) N J H Holroyd and D Hardie, Corrosion Science 21, pp 124-144 (1981)

(39) L B Vogelsang and J Schijve, Fatigue of Engineering Materials and Structures 3, pp 85-98 (1980)

(40) A H Hamish and L H Burk, NACE 38 No 6 (1982)

(41) T L Gerber and H O Fuchs, Journal of Materials, Vol 3, pp 359-74 (1968)

(42.) R P Hubbard, Journal of Basic Engineering, Transaction of ASME, pp 625-31 (Dec. 1969)

(43.) H Saal, Journal of Basic Engineering, Transaction of ASME, pp 243-47 (March 1972)

(44) R Hermann and C N Reid, Effects of Residual Stresses on the Fatigue of AA 7017 in Moist Air, presented paper at the International Conference of Materials and Structures, Freiburg, West Germany, June 20-24 (1983)

(45) R E Swanson, A W Thomson, J M Bernstein and J L Malony, Hydrogen Effect in Metals, ed. J M Bernstein and A W Thomson, Pittsburg USA, 460 (1981)

(46) ASTM Standard, British Standard BS 5447 (1977)

(47) C N Reid, private communication (1983)

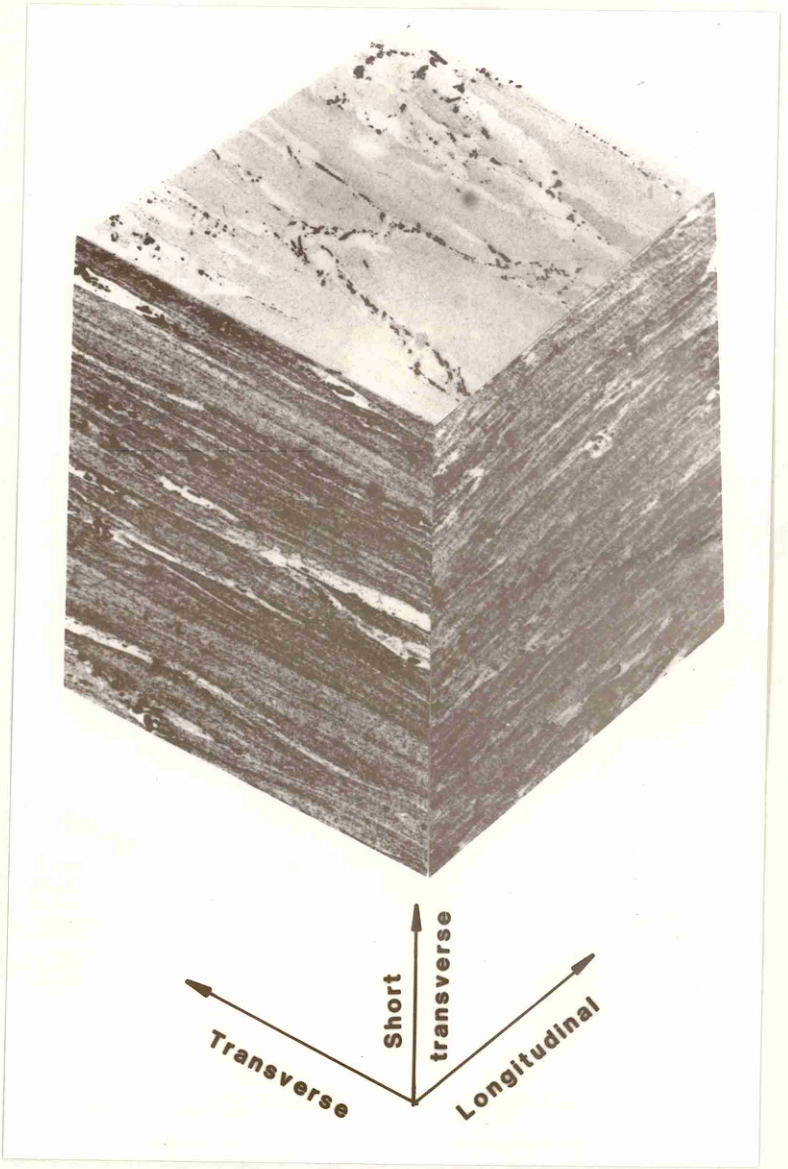

Fig 1 Microstructure of the aluminium alloy 7017-T651 indicating longitudinal, transverse and short directions

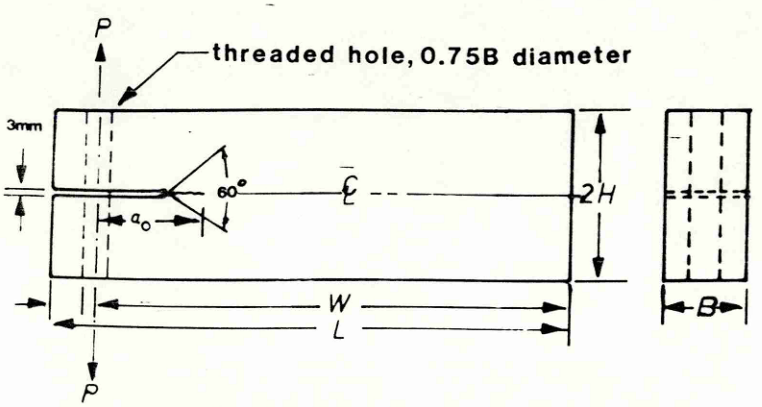

Fig 2a Geometry of the Double-Cantilever-Beam (DCB) specimen

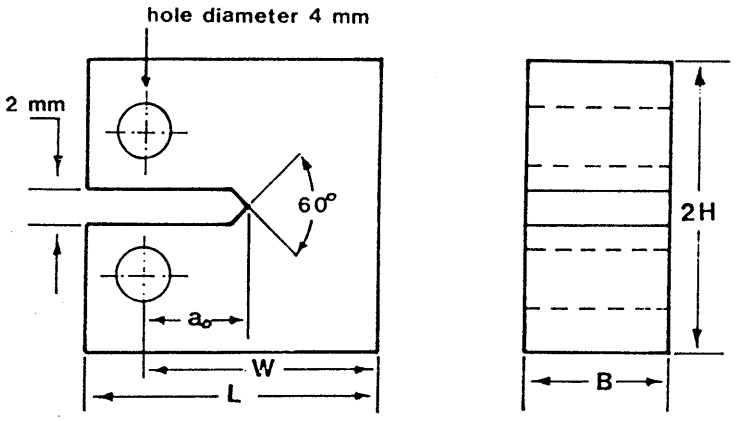

Fig 2b Geometry of the compact-tension specimen

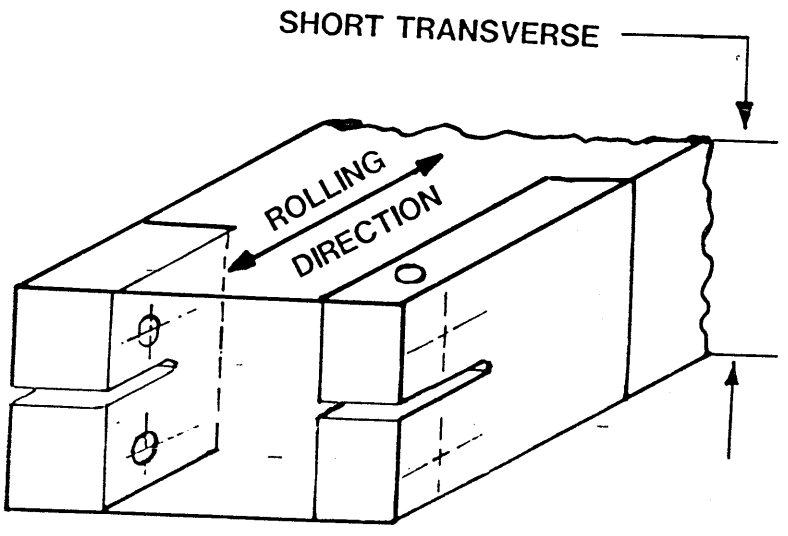

Fig 3 Rolling direction and orientation of plate from which test specimens are made

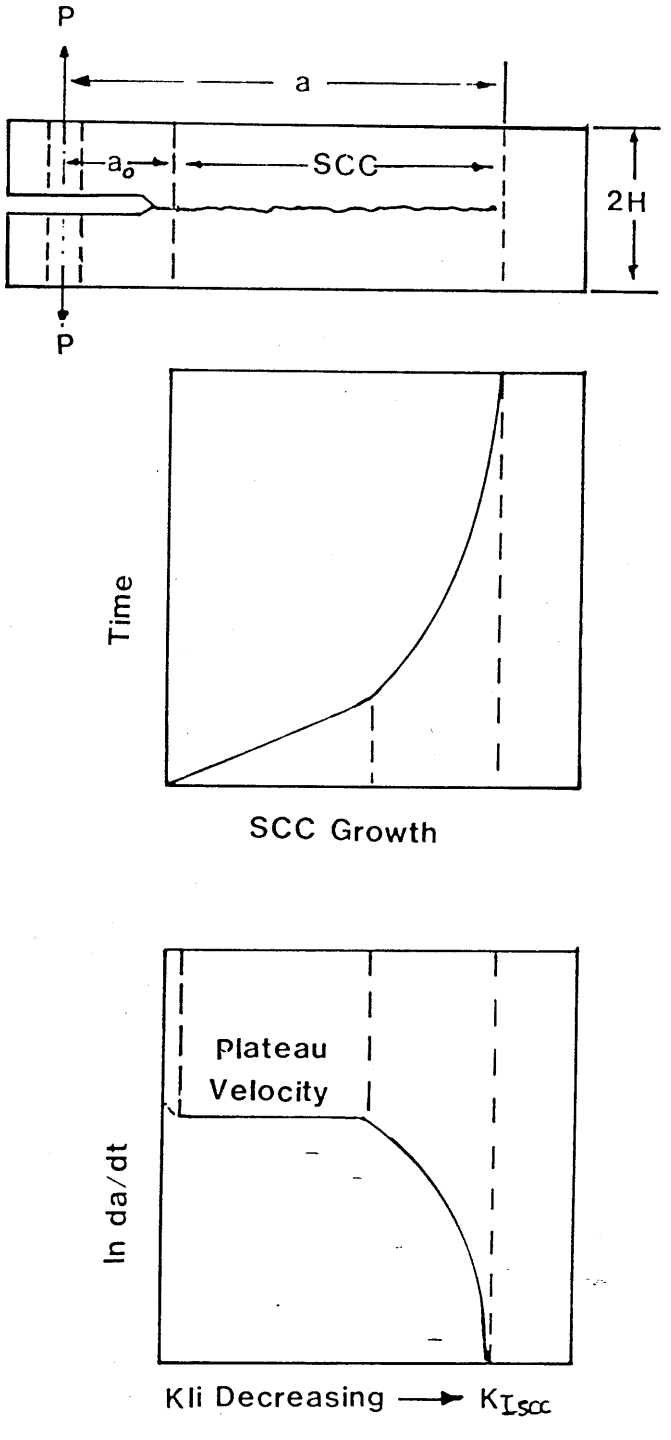

Fig 4 Schematic event of Stress-Corrosion-Cracking in a DCB specimen

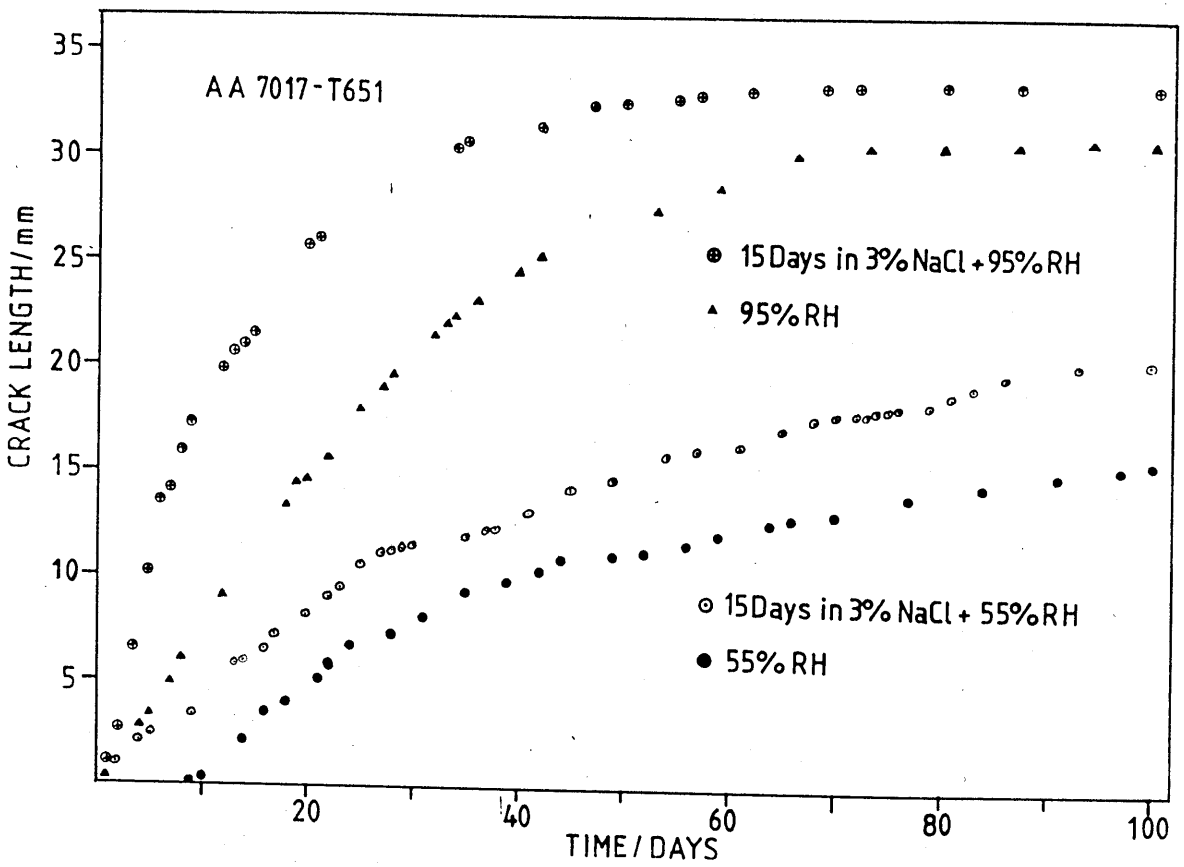

Fig 5 Crack extension versus time curves for various environments

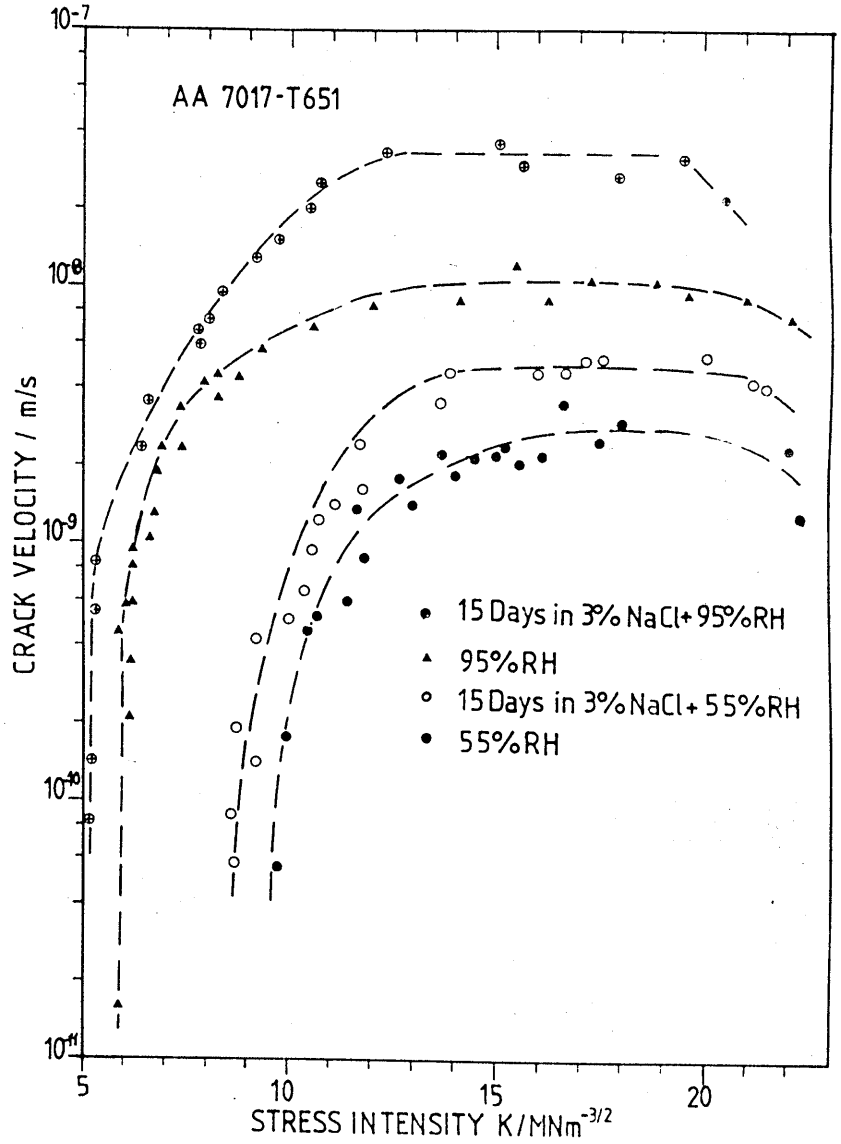

Fig 6 Log of crack velocity versus stress intensity showing the effect of the environment from data of Fig 5

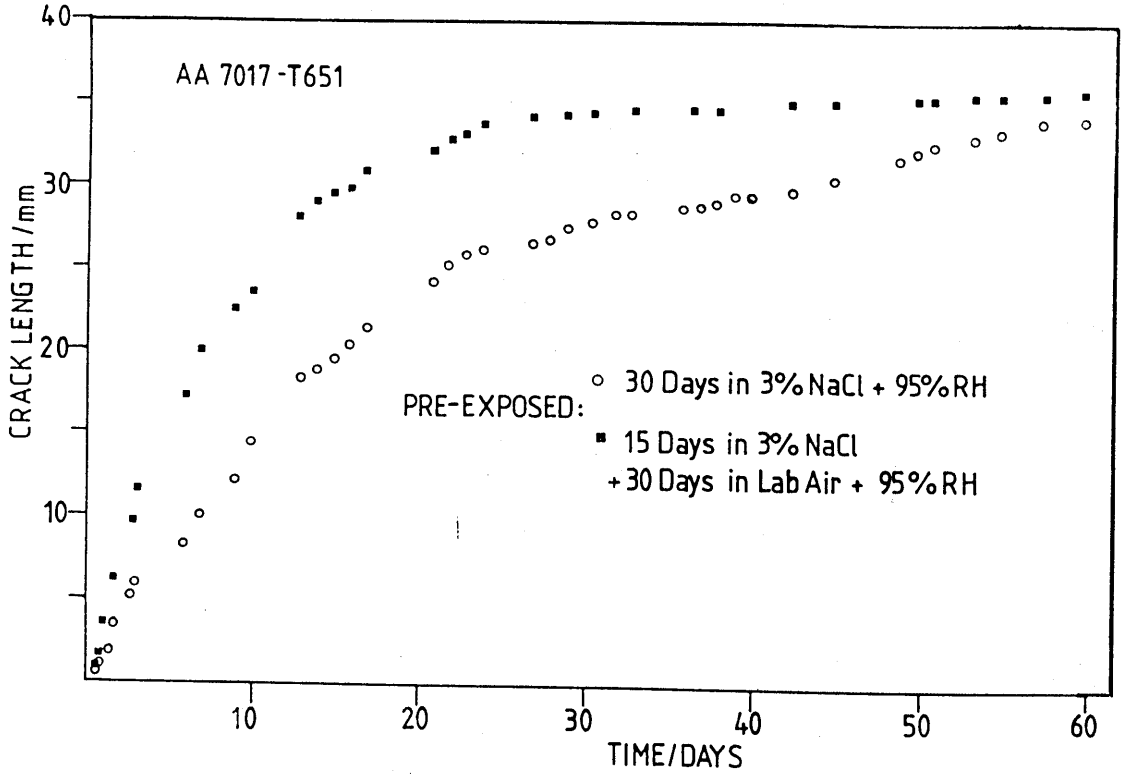

Fig 7 Crack extension versus time curves for pre-exposed alloy in two different environments

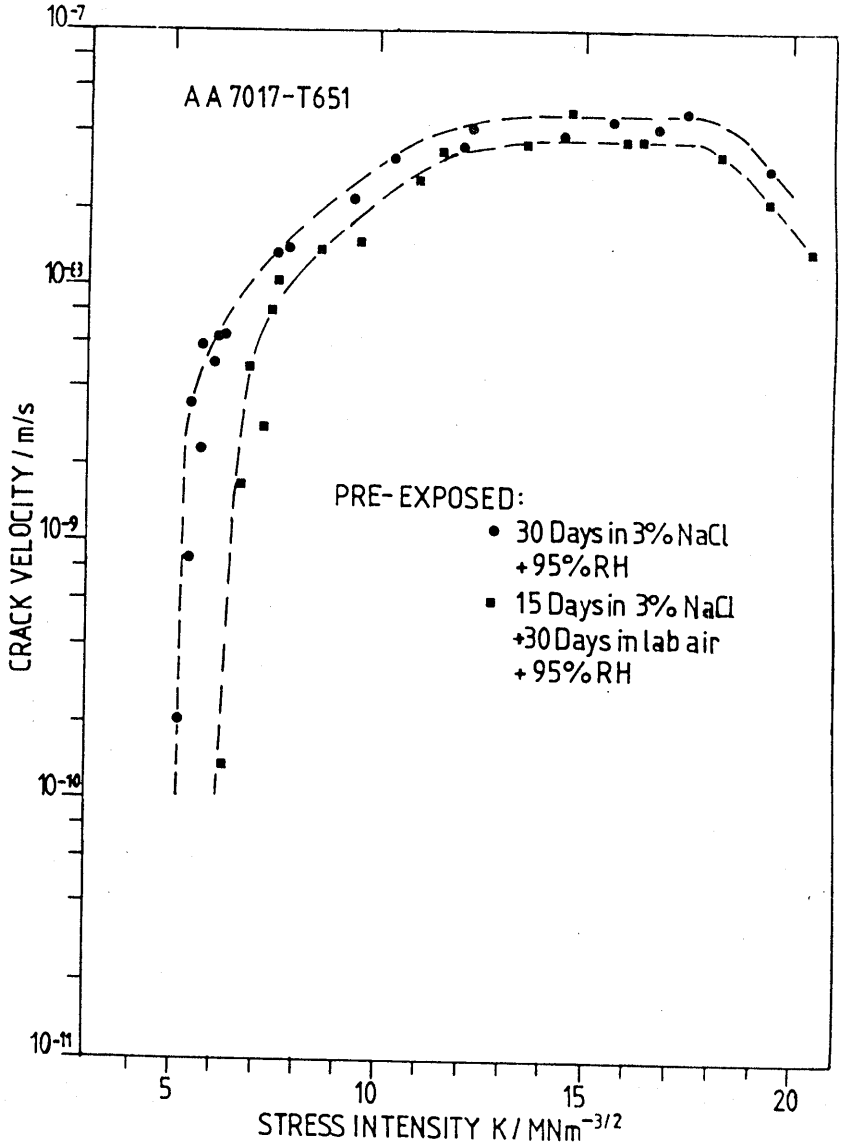

Fig 8 Log of crack velocity versus stress intensity drawn from data of Fig 7

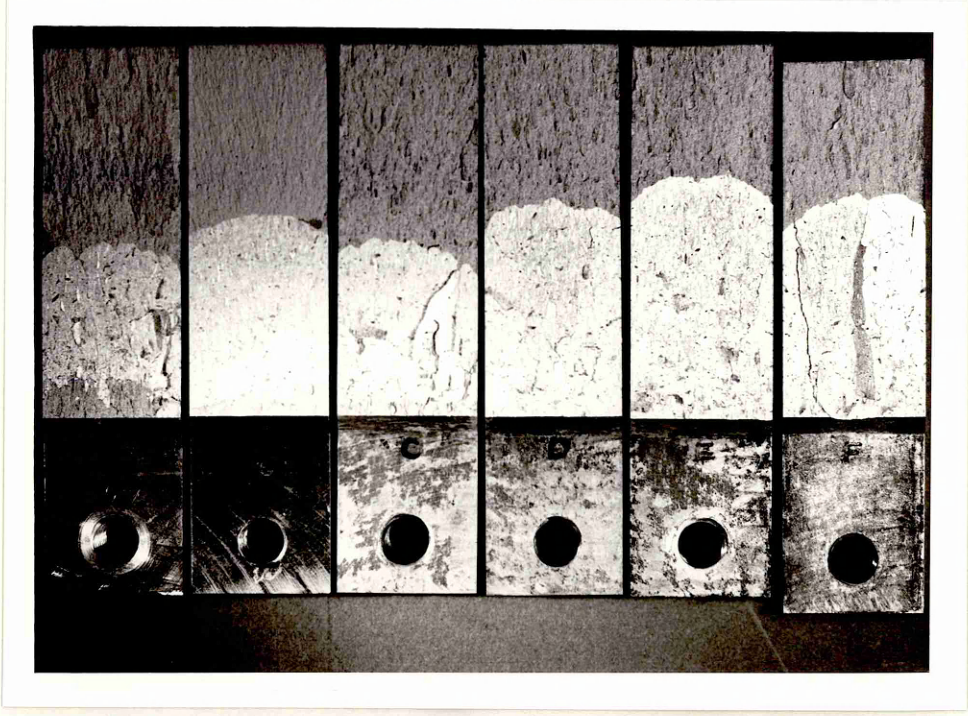

Fig 9a View of SCC fracture surfaces for test environments A-F (from left A to right F).

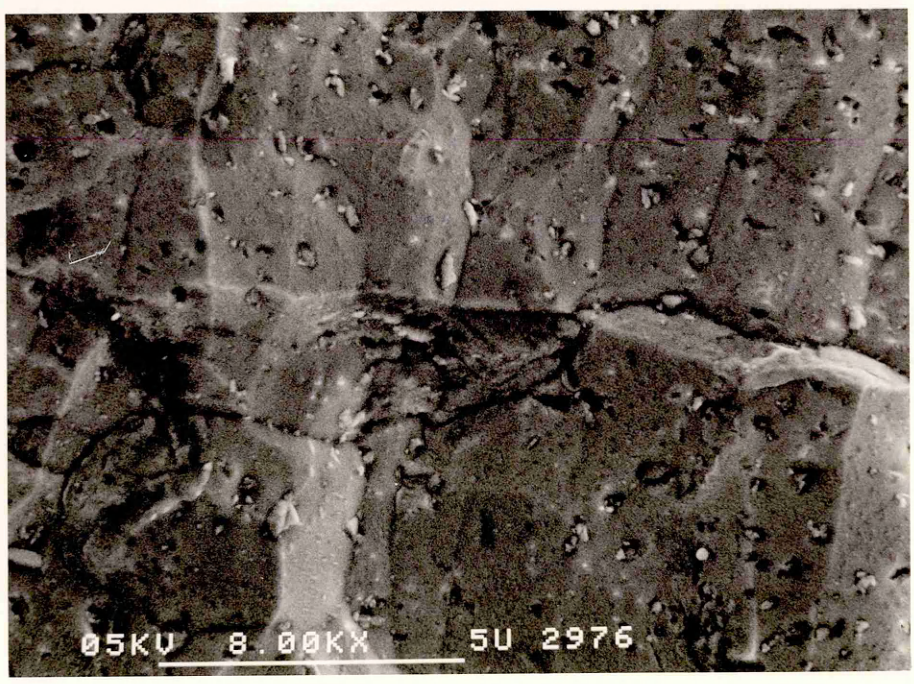

Fig 9b SEM Micrograph revealing the intergranular nature of fracture, also evident are a number of intermetallic particles. Micrograph taken from Region II of the fracture surface and stress corroded in 95% RH (Environment B).

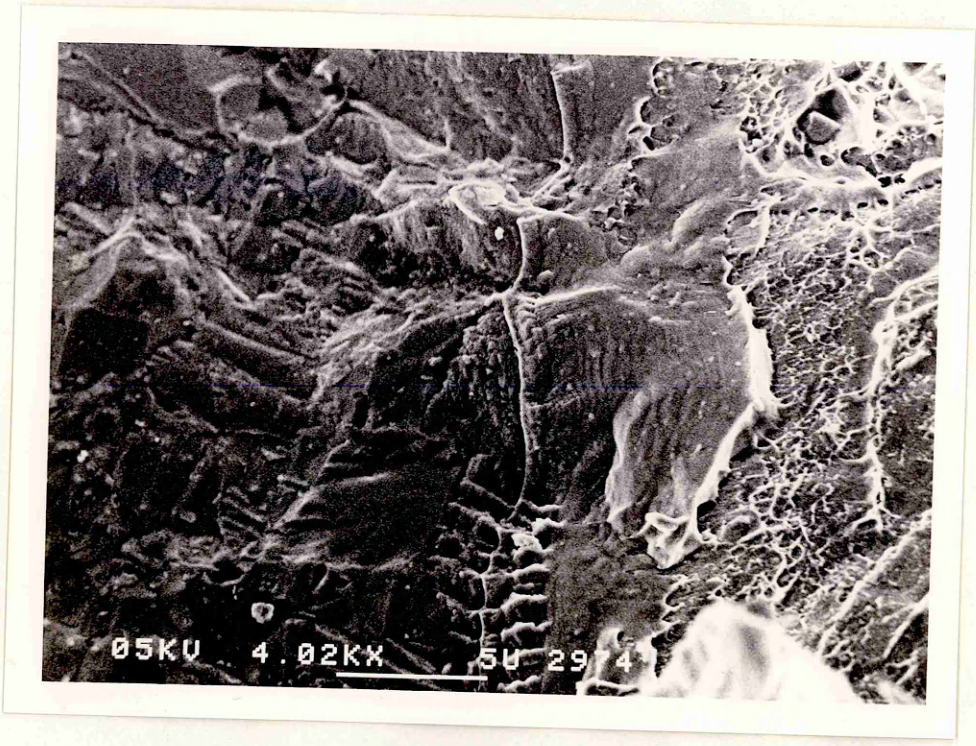

Fig 9c Similar fracture appearance to 9b, obtained from fracture of Region I. The Crack Propagation Direction (CPD) is from left to right.

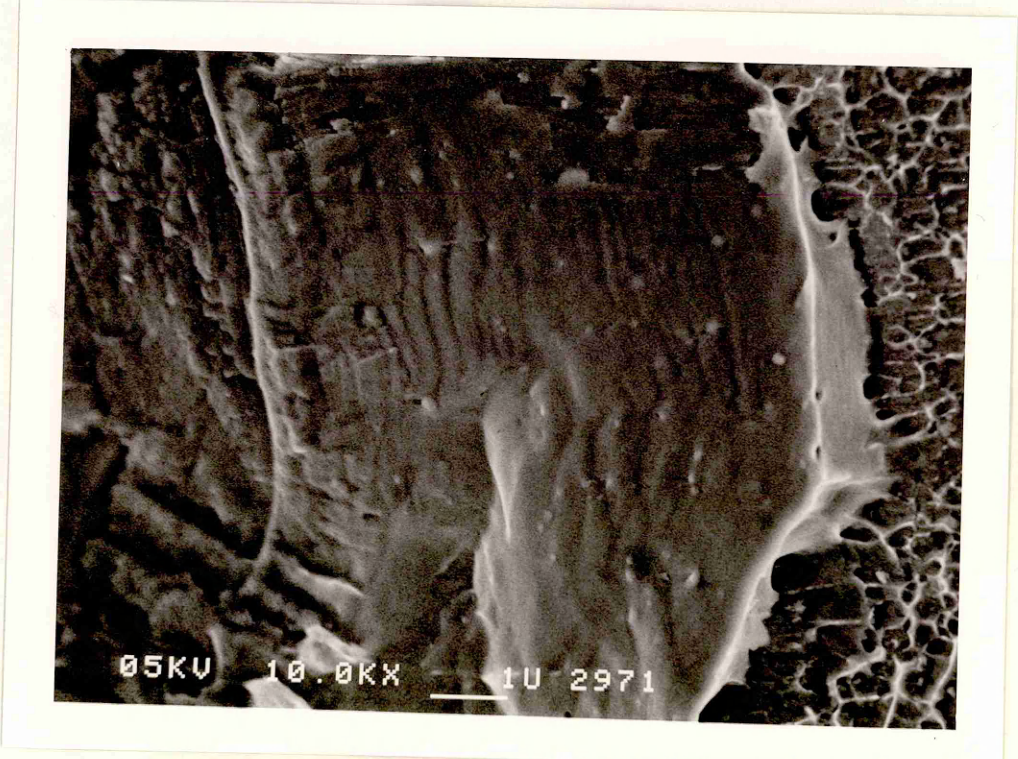

Fig 10 High magnification of fracture near the crack tip, same area as 9c, CPD from left to right.

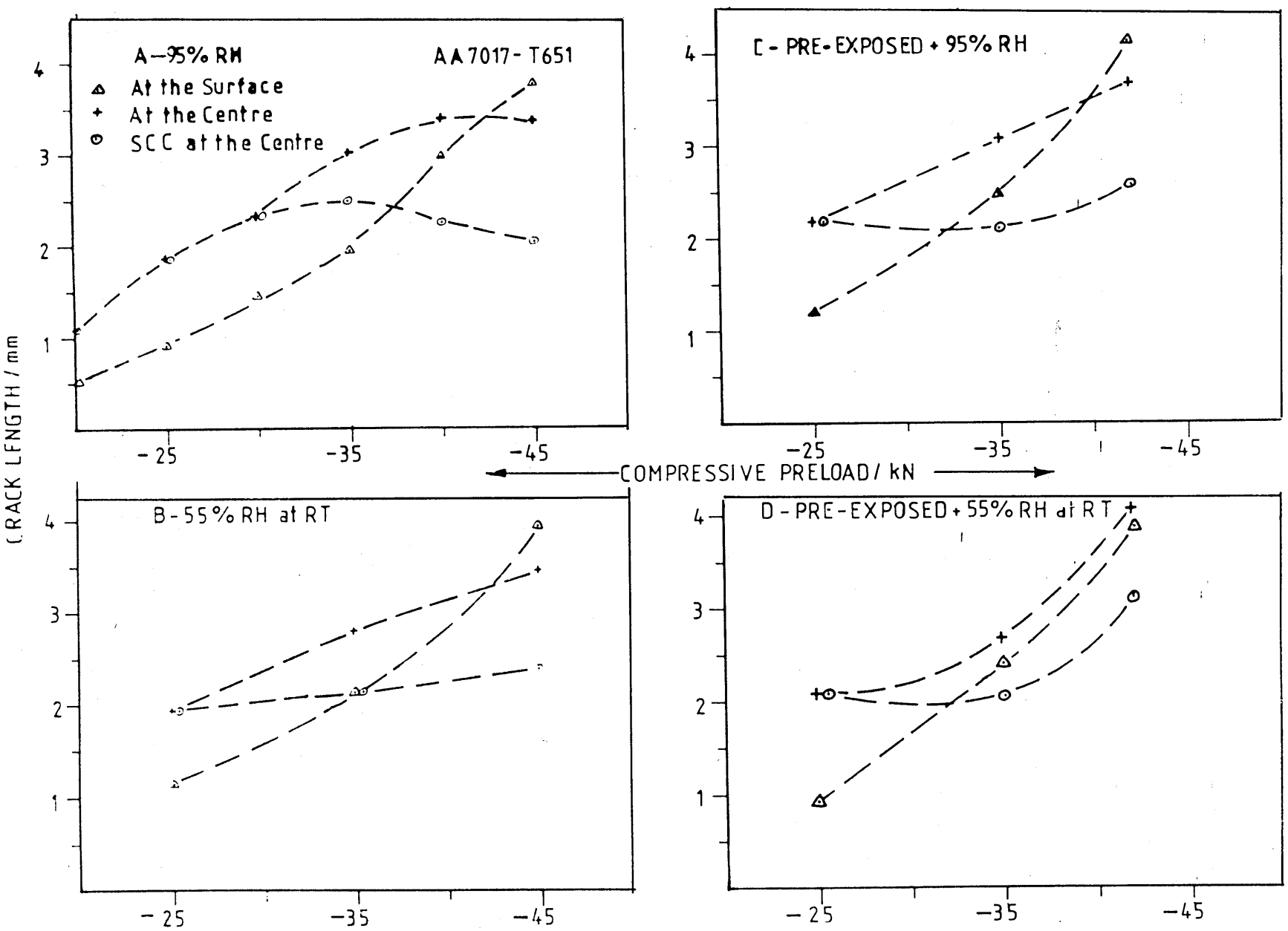

Fig 11 a - d Crack extension versus compressive pre-load as a function of environments, test A - D

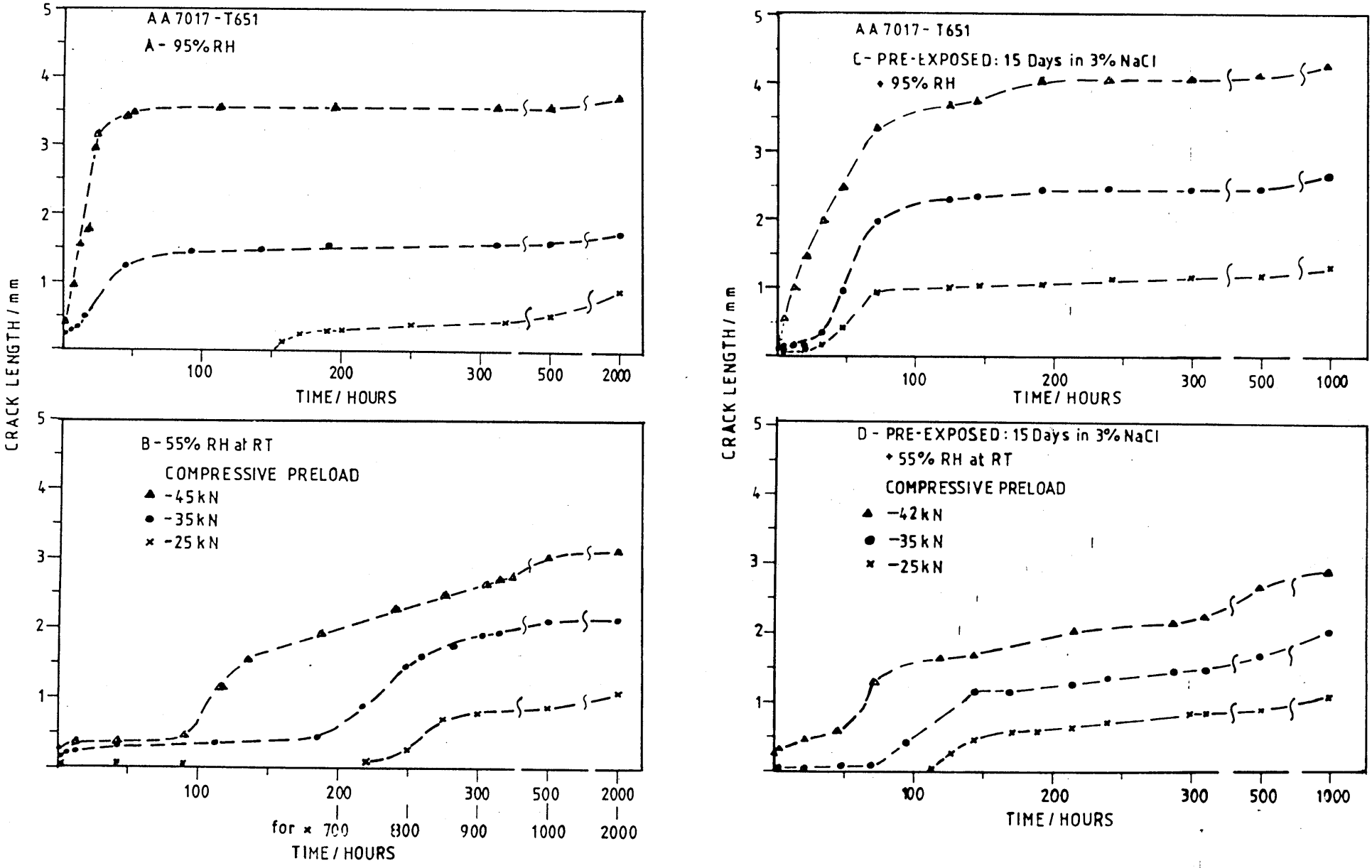

Fig 12 a - d Crack extension versus time showing the crack growth on pre-load and environment

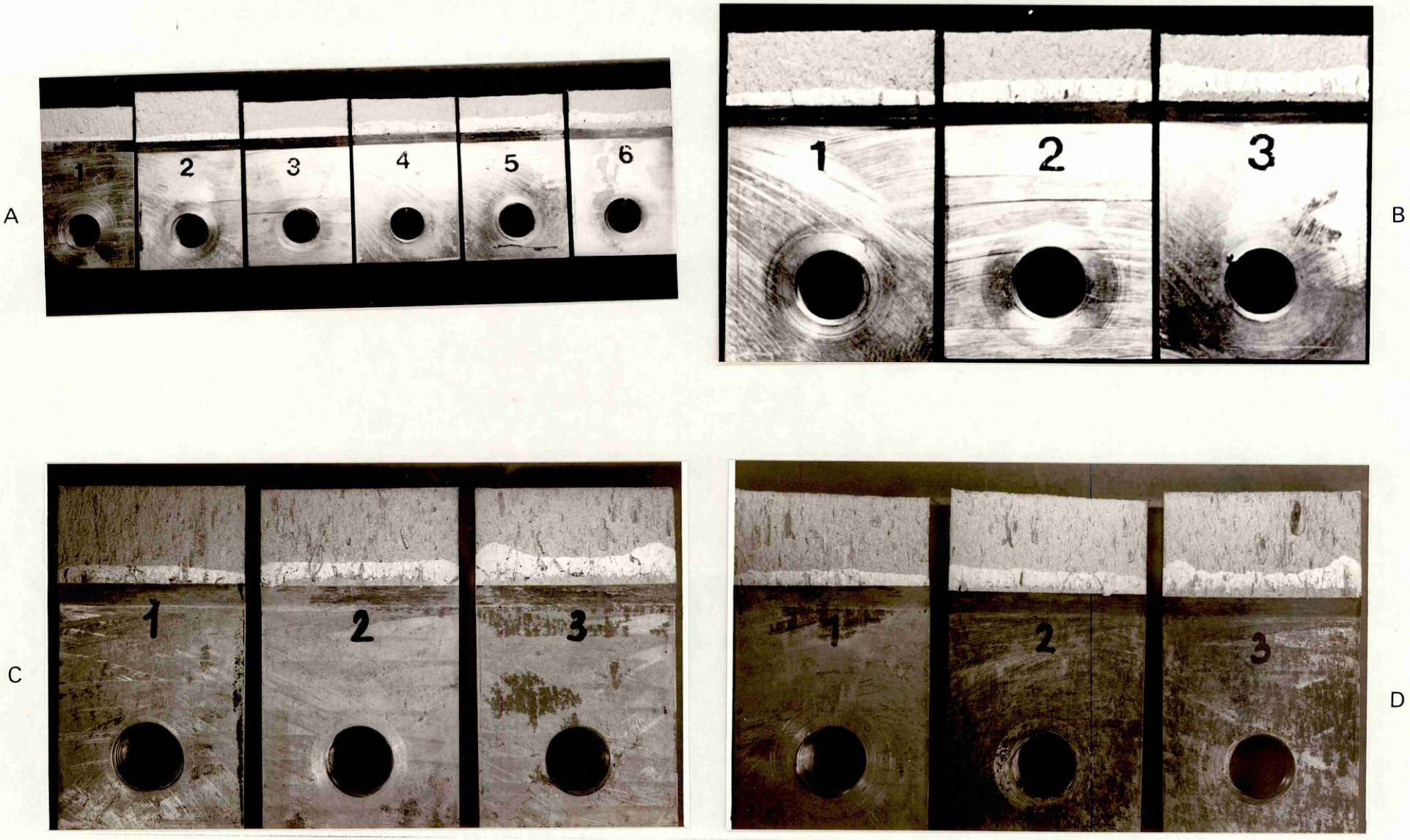

Fig 13 Macroscopic view of fracture surfaces for various pre-loads and environments; A - 95% RH, B - 55% RH, C - pre-exposed + 95% RH and D - pre-exposed + 55% RH

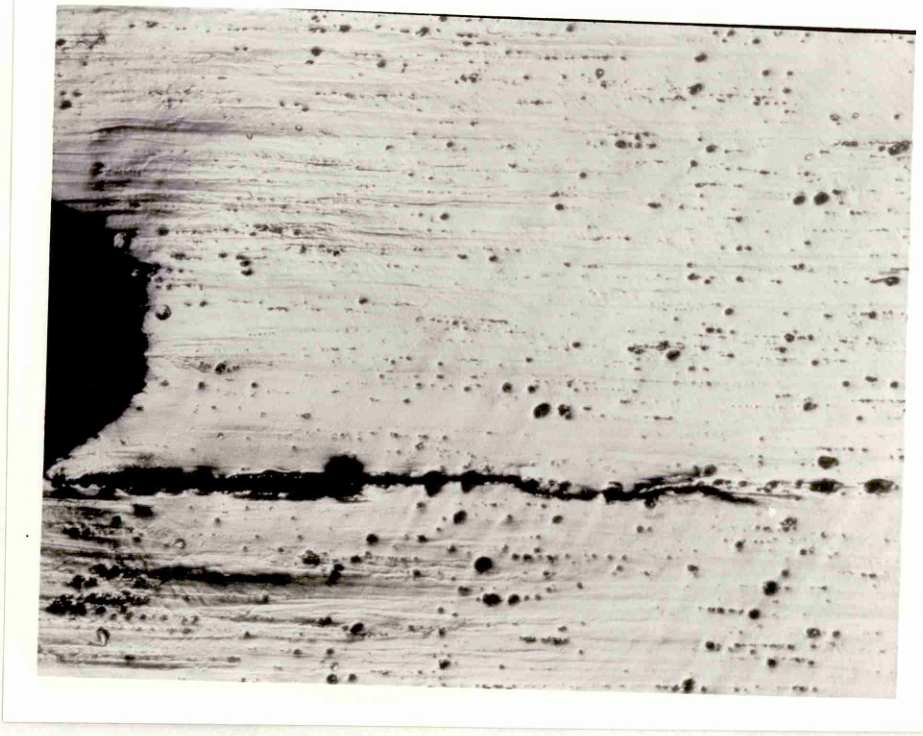

Fig 14 Specimen surface after application of -45 kN pre-load and unloading. A crack is formed within a few minutes of unloading following a parallel line of inclusions. Note heavily distorted surface around the notch and slip bands that lie at approx. 45° to the crack

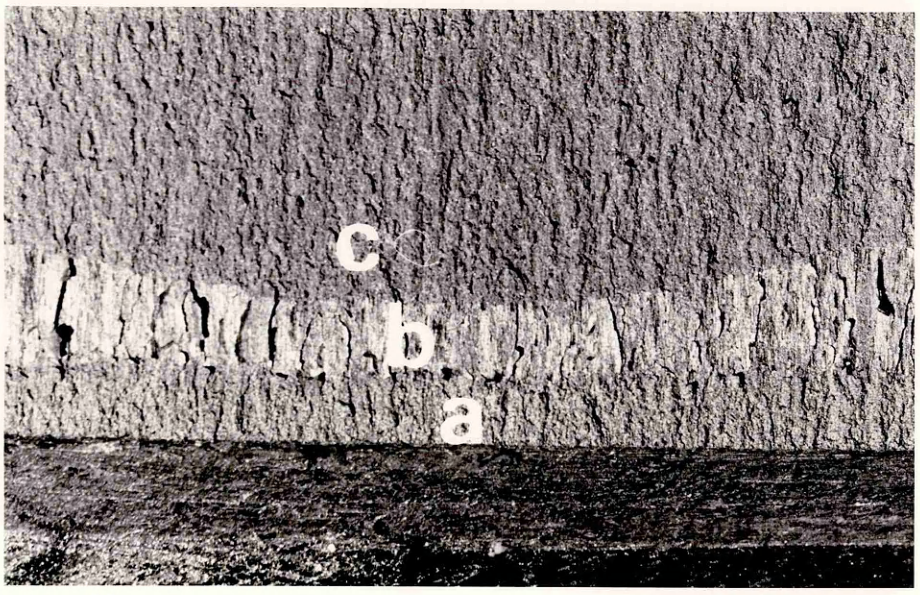

Fig 15 Magnified view of the same fractured specimen, pre-loaded to -45 kN and exposed to 95% RH. Region 'b' is the stress corroded surface.

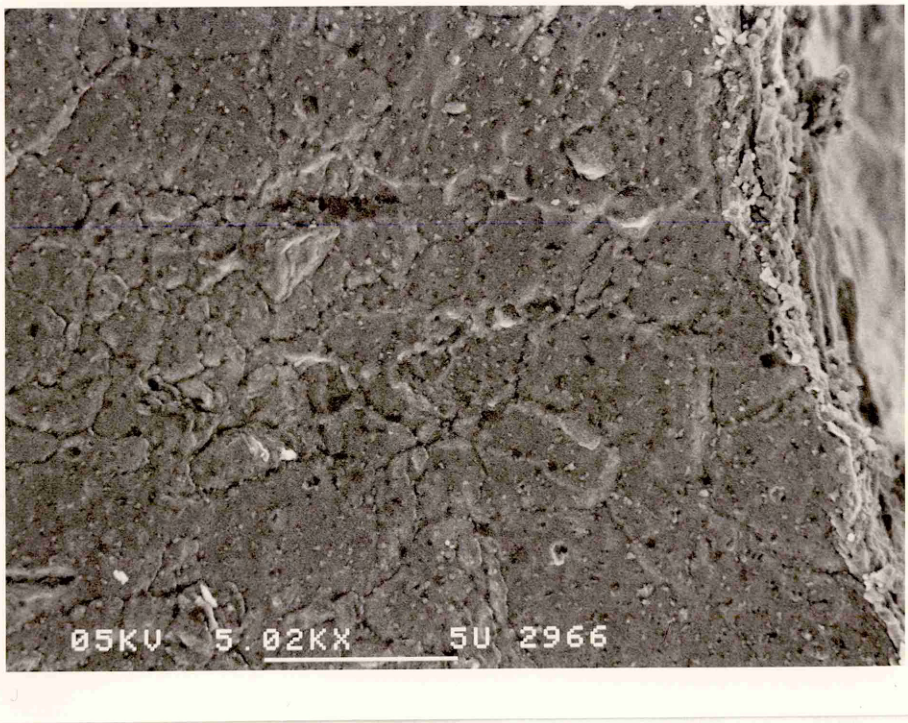

(a)

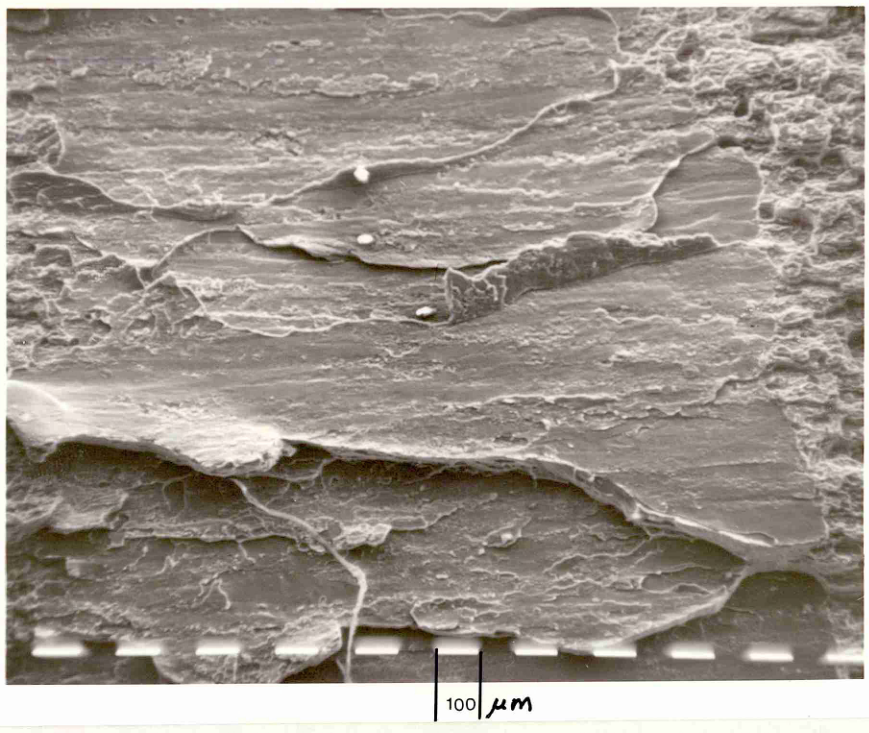

(b)

Fig 16 a and b High and low SEM micrographs showing the intergranular nature of fracture (a) and steps and terraces in (b); CPD is from right to left.

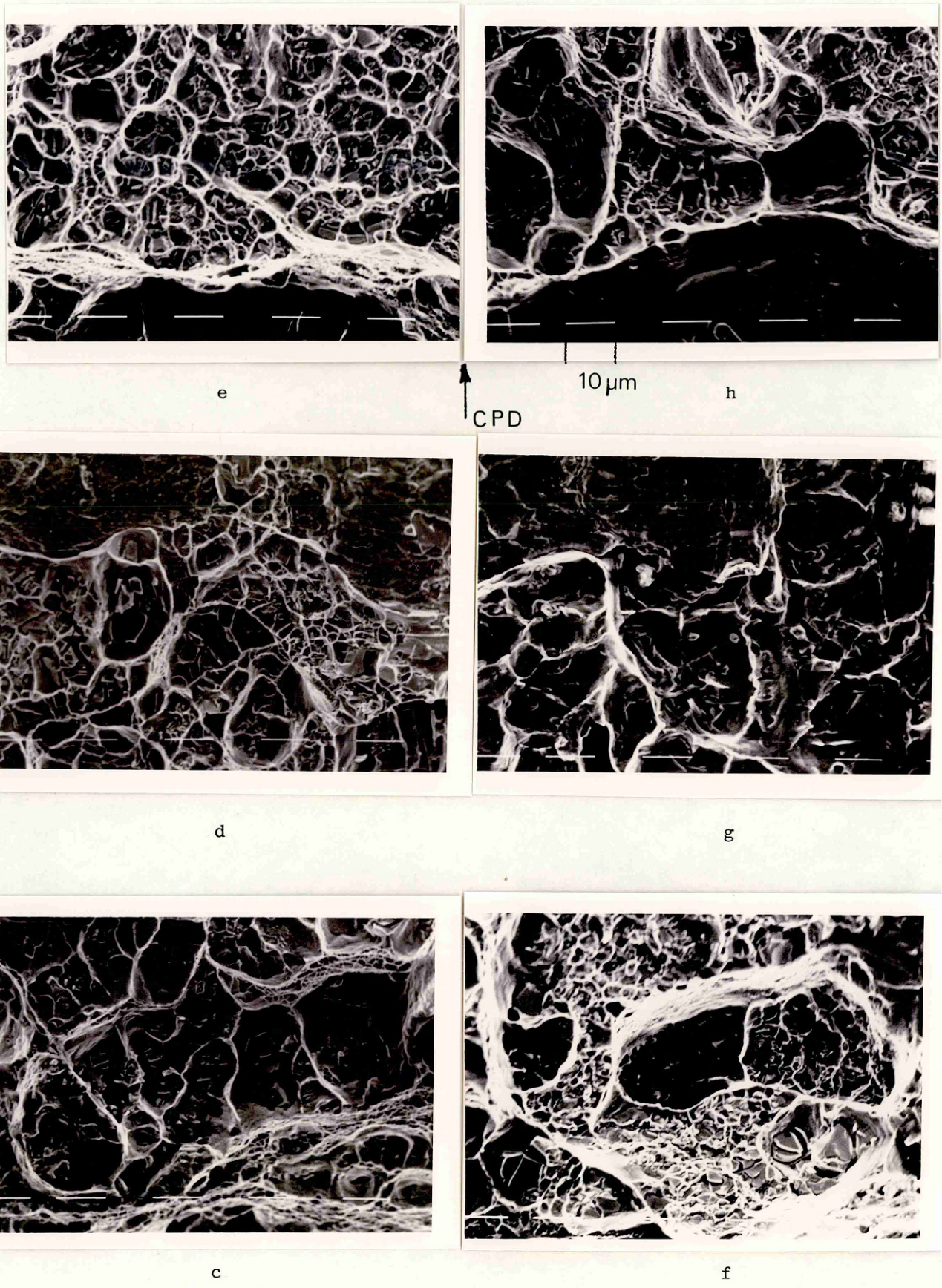

Figure 16 c - e morphologies of unexposed alloy, f - h for pre-exposed alloy

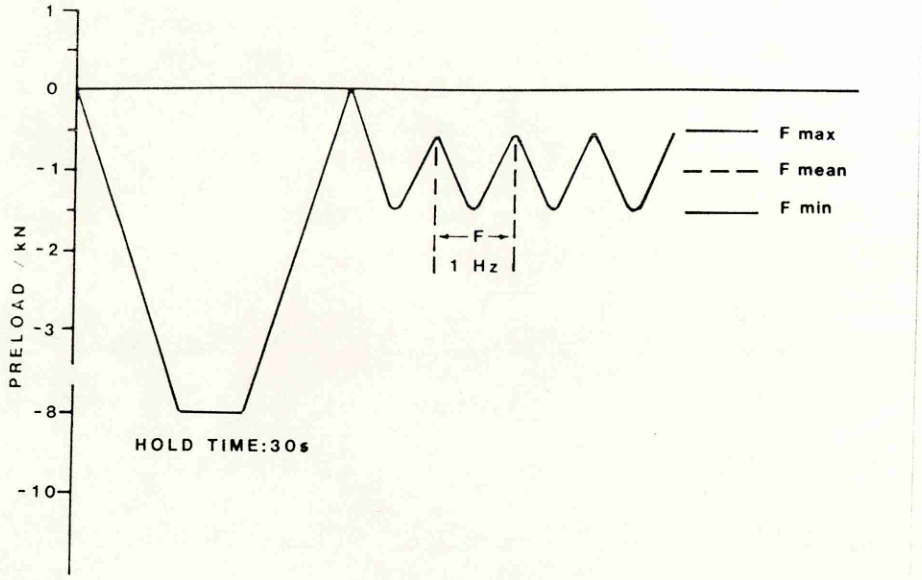

Fig 17 Schematic event of compressive pre-loading, unloading and fatigue loading for miniature CT specimens

Fig 18 Brittle lacquer applied to the surface of the specimen revealing a residual tensile stress field surrounding the notch tip

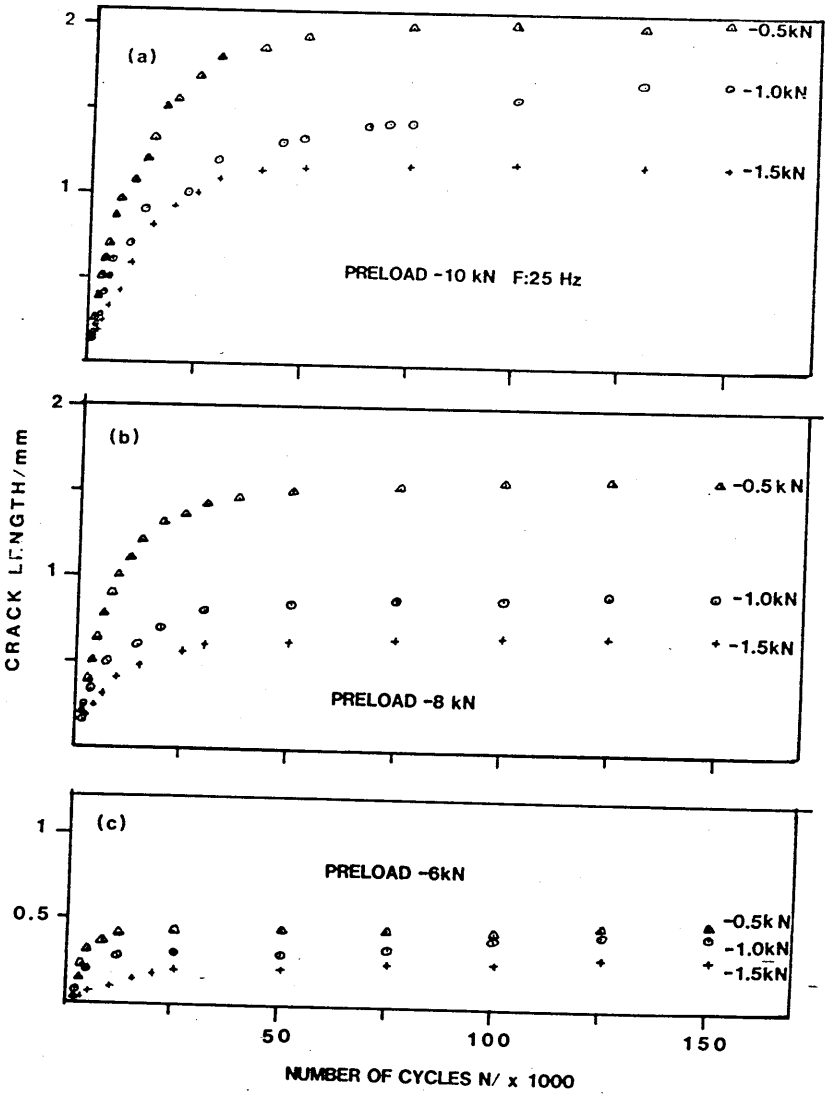

Fig 19 (a,b,c) Crack length versus number of cycles for specimens pre-loaded to -10 kN (a), -8 kN (b) and -6 kN (c) for 25 Hz

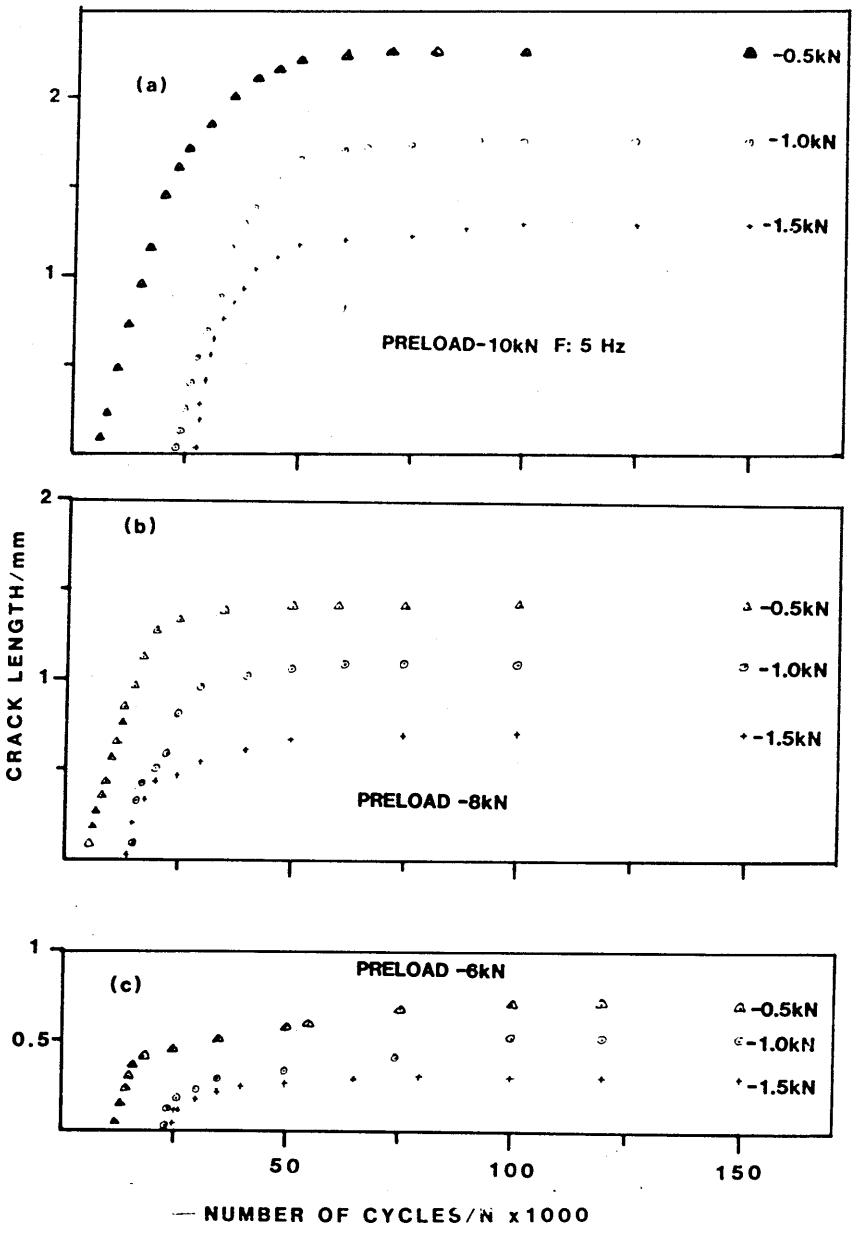

Fig 20 (a,b,c) As Fig 19 but for 5 Hz

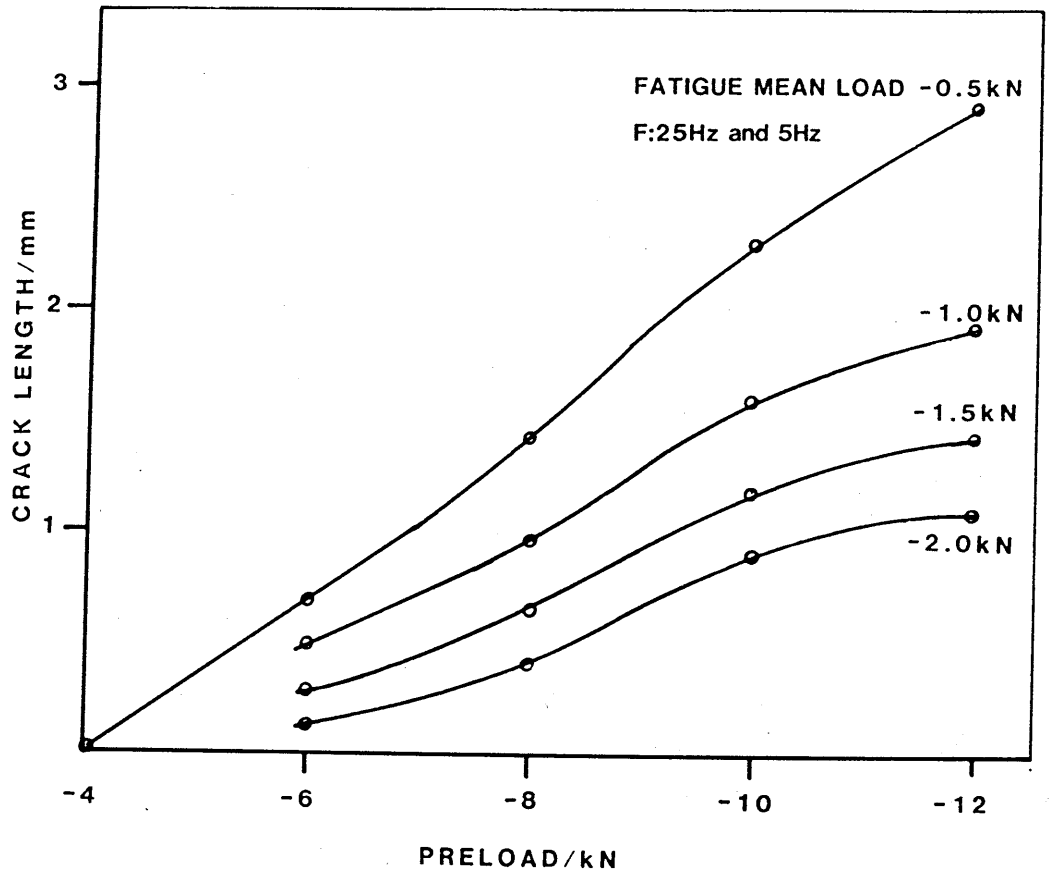

Fig 21 Final crack length plotted against compressive pre-load as a function of mean load, -0.5 to -1.5 kN for 25 Hz and 5 Hz

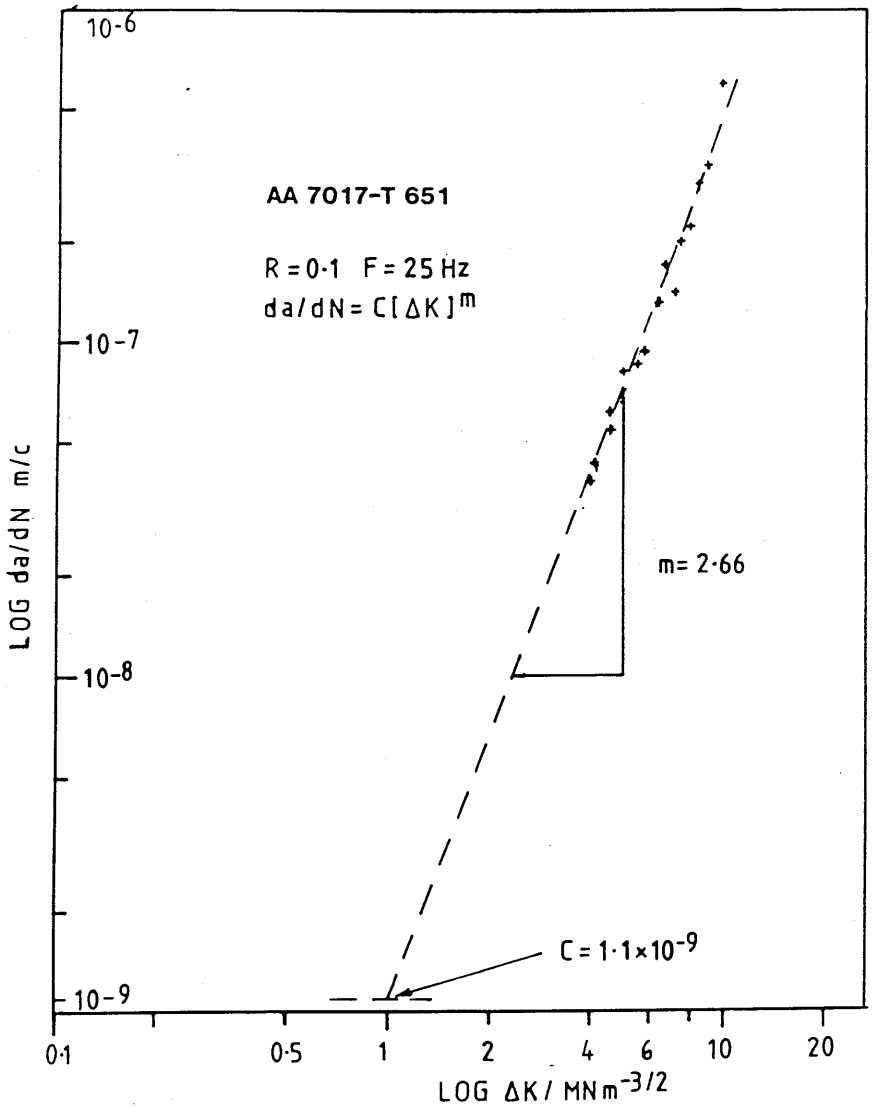

Fig 22 Crack growth rate log da/dN as a function of log ΔK to determine the constant C and exponent m, frequency 25 Hz, R ratio 0.1, tension-tension fatigue in lab air, 54% RH

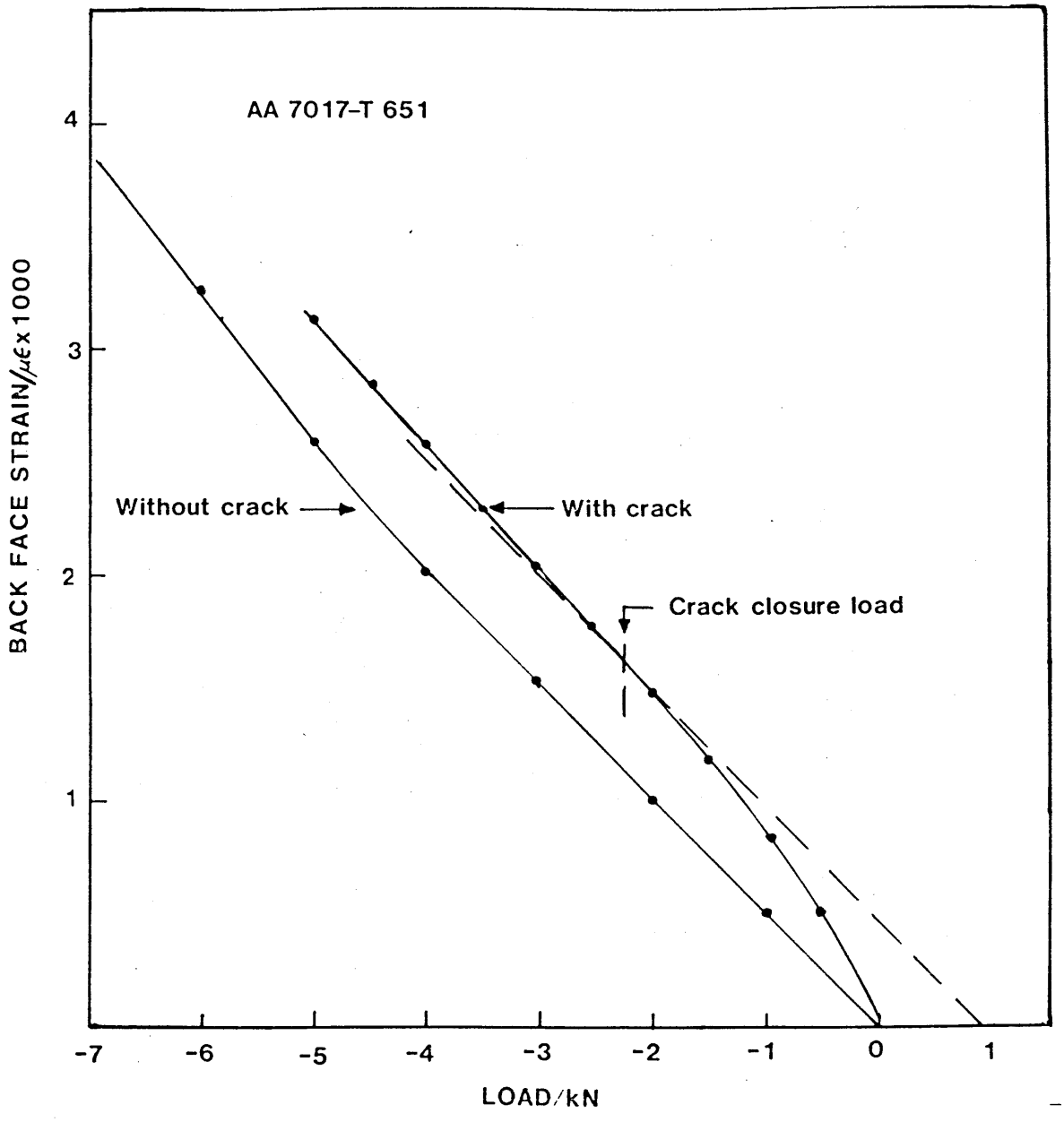

Fig 23 Compliance graph of Back face strain plotted against compressive pre-load for uncracked and cracked specimen

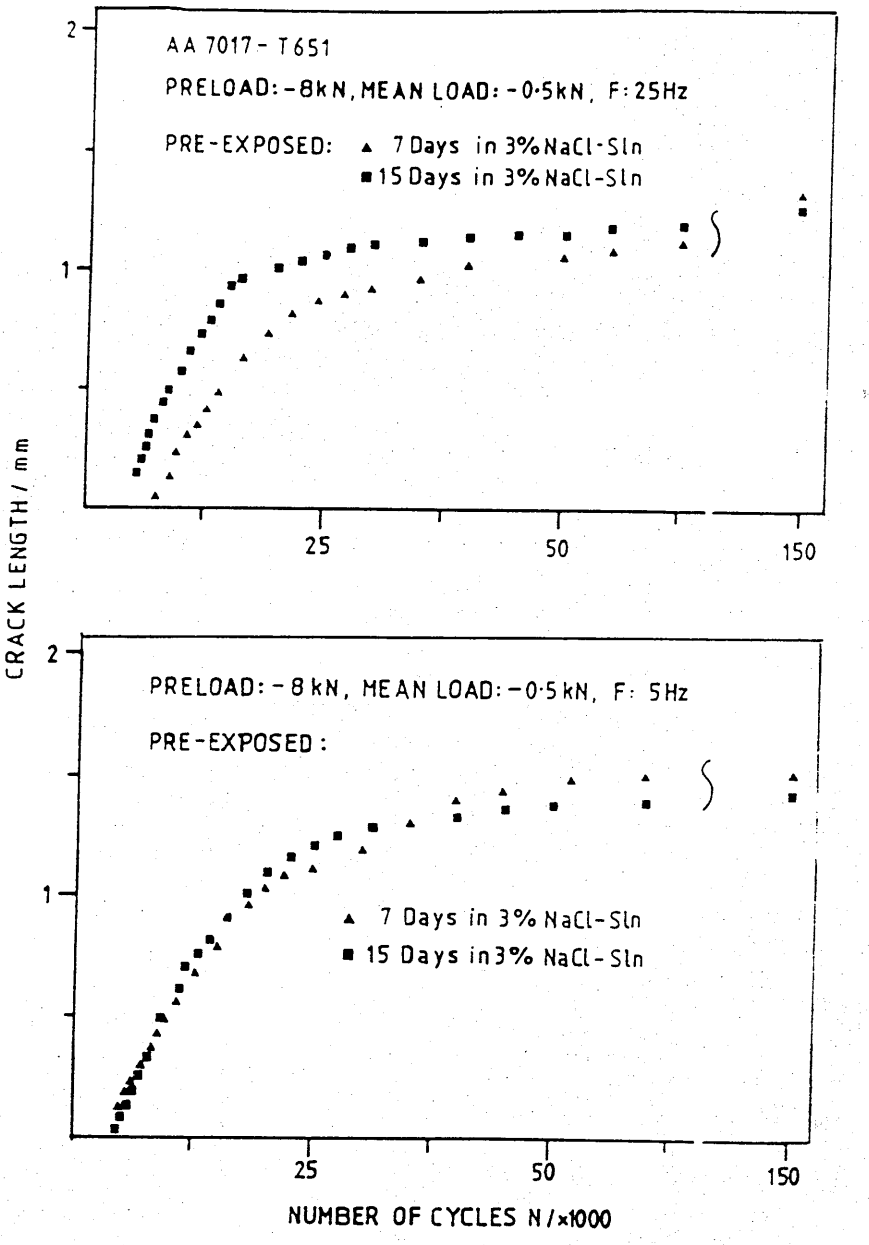

Fig 24 (a,b) Crack length a versus number of cycles N for specimen pre-soaked in salt solution for 7 and 15 days prior to compressive pre-loading and cycling at a mean load of -0.5 kN; F = 25 and 5 Hz

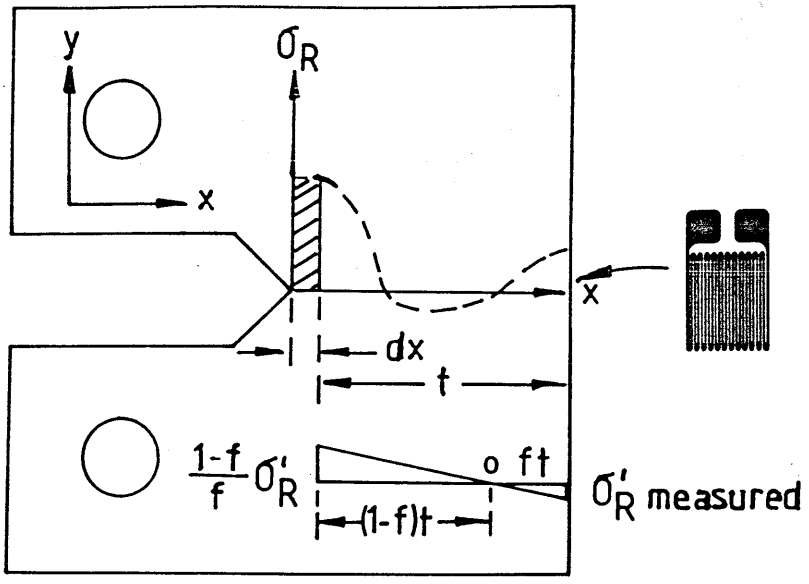

Fig 25 Compact Tension Specimen showing dimensions to determine force and moment equilibria.

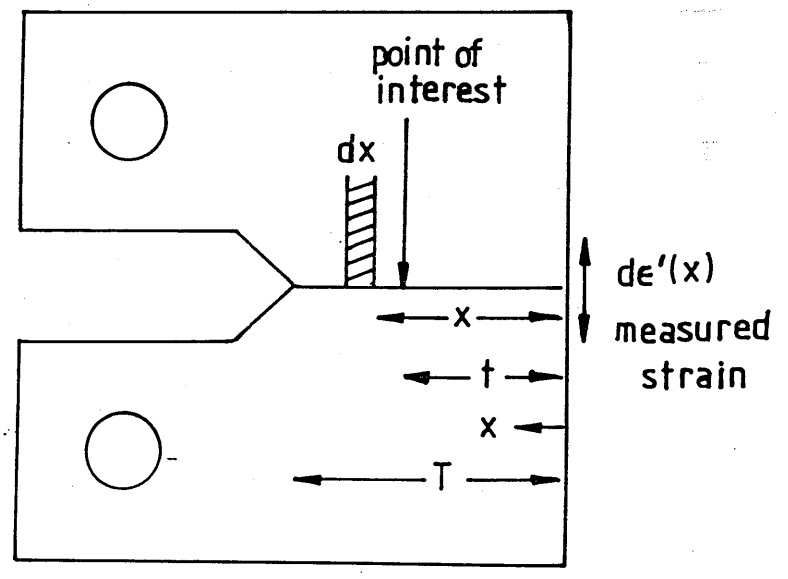

Fig 26 Same specimen showing dimensions to determine the residual stress distribution

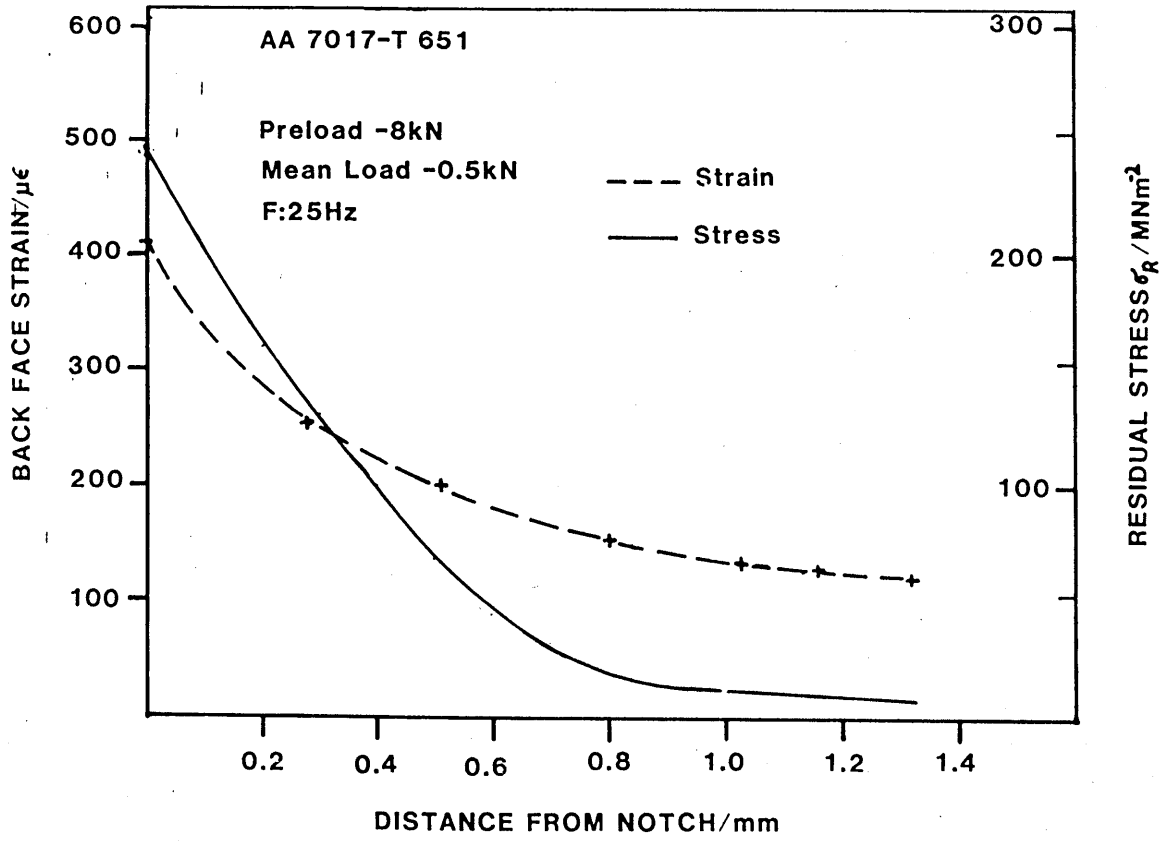

Fig 27 Residual Stresses determined from back-face strain measurements in CT specimens

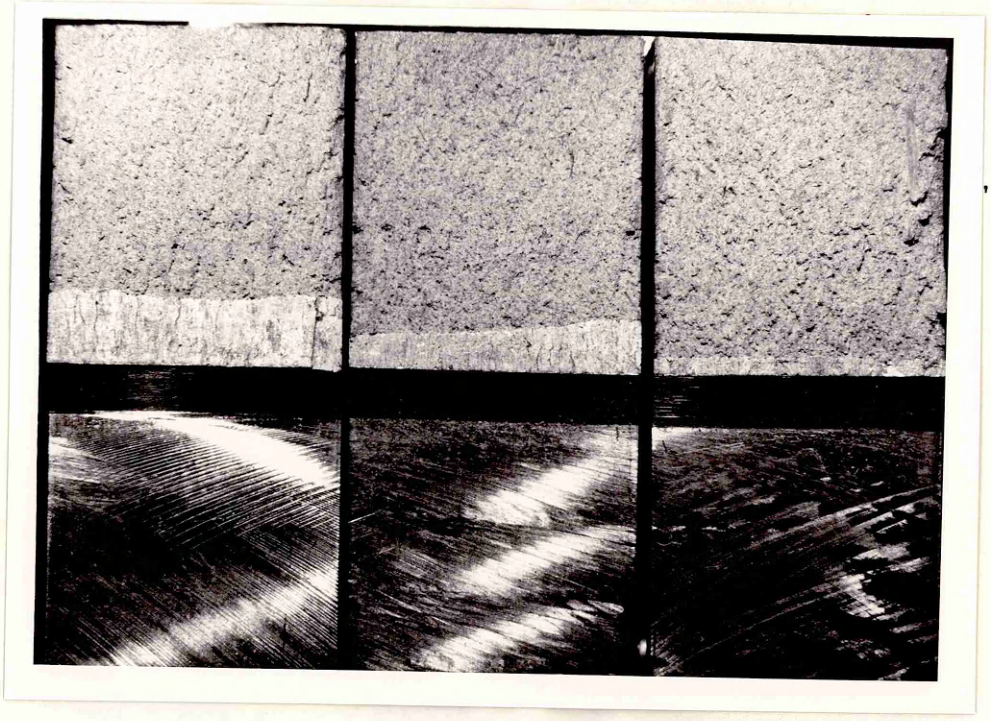

Fig 28 Optical micrograph of specimens fatigued with 25 Hz, from left to right - compressive load -10, -8 and -6 kN, mean load ±0.5 kN

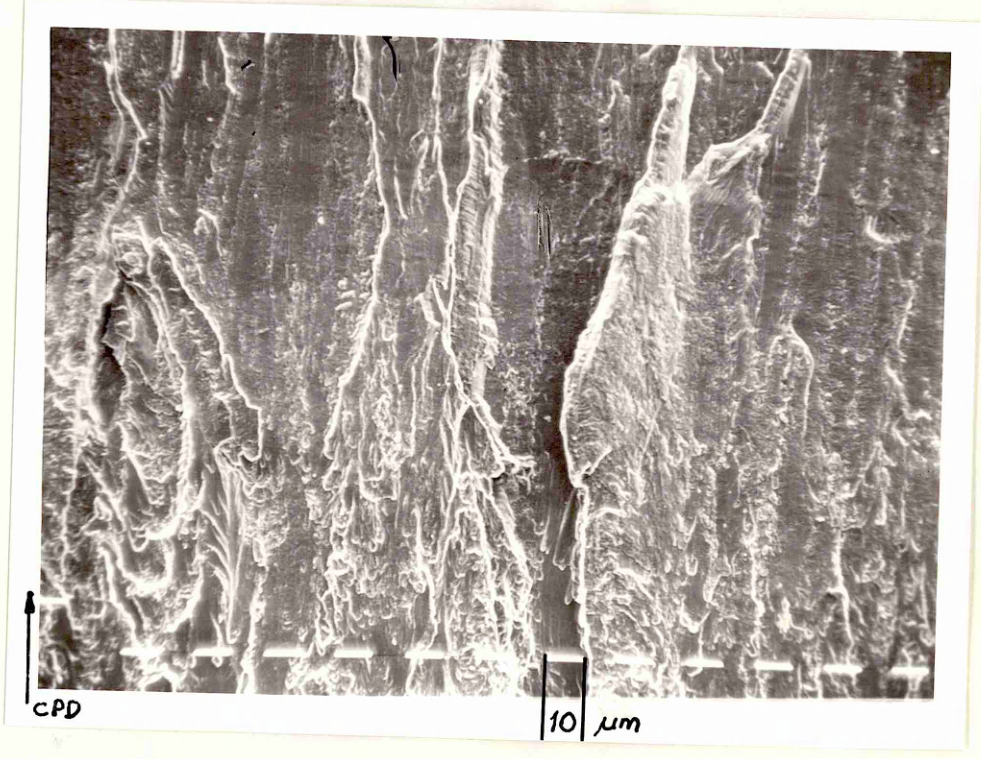

Fig 29 (a - d) SEM micrographs showing the fracture morphology of the fatigue crack a), cracking initiated from the root of the notch b), appearance at midway of fracture c) and at the end of the fatigue with the overload break-open fracture at the top d).

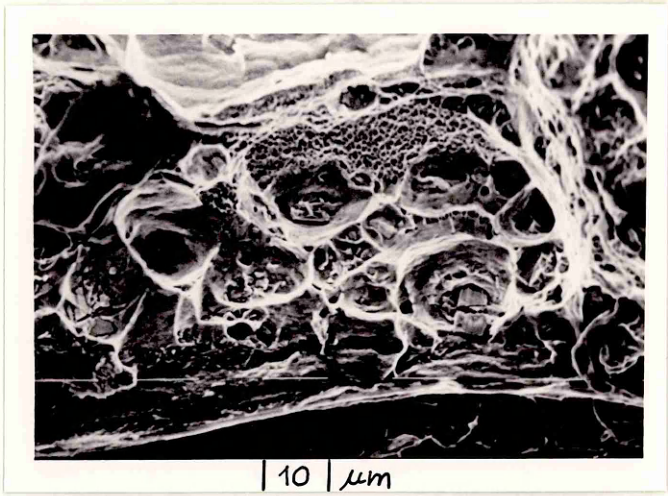

Fig 29 b)

Fig 29 c)

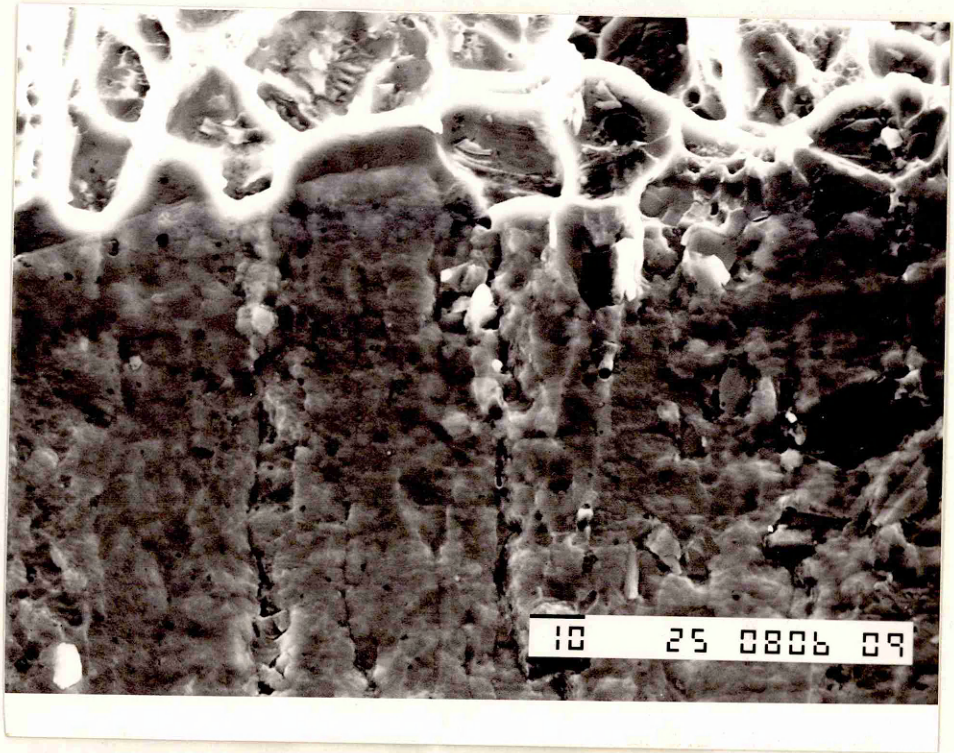

Fig 29 d)

Fig 30 a) SEM micrograph of 7 day pre-exposed specimen fatigued at 25 Hz, mean load ± 0.5kN

b) higher magnification showing the nature of embrittlement

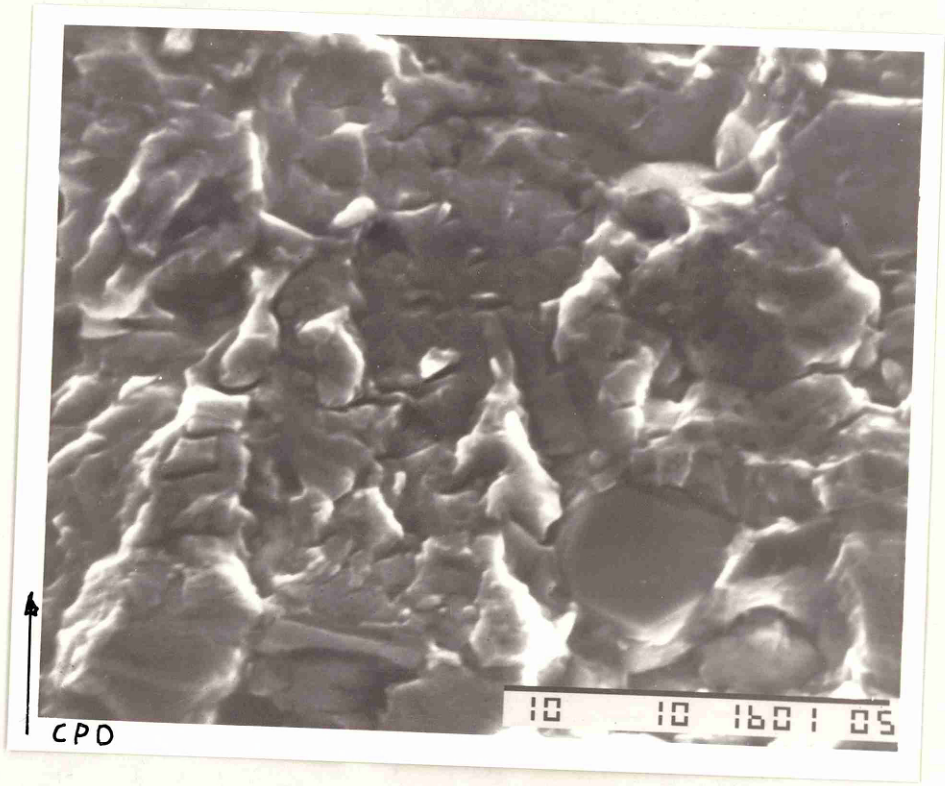

Fig 30 b)

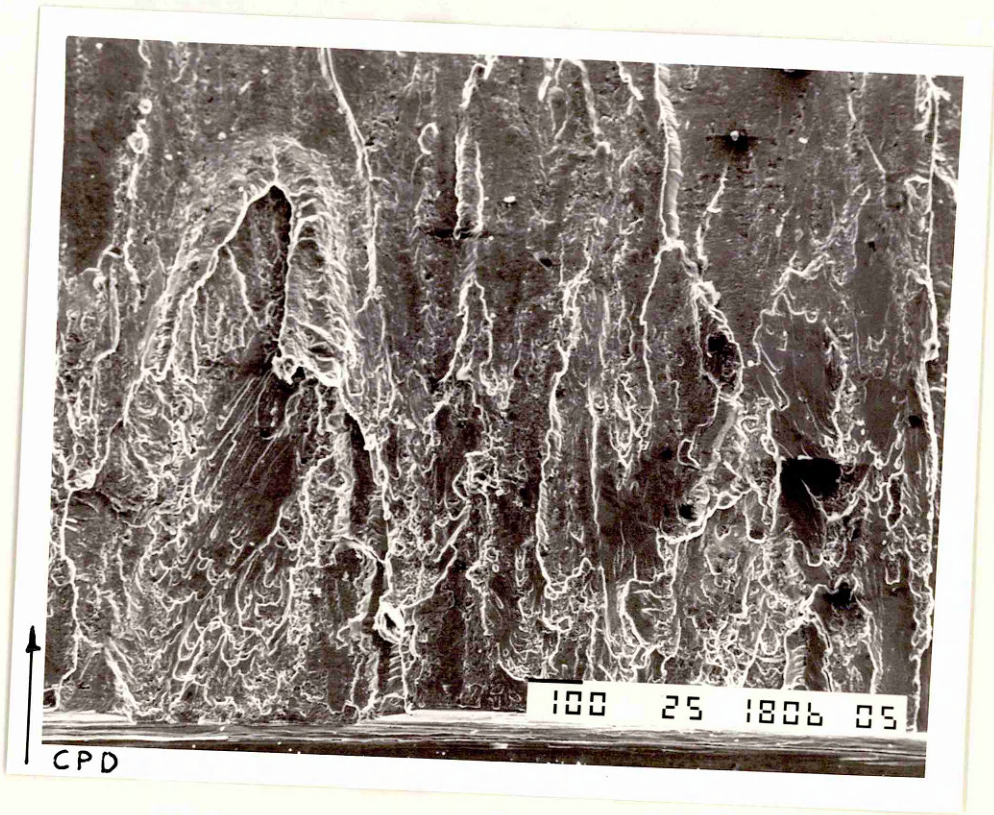

Fig 31 a) SEM micrographs as above but fatigued at 5Hz

b) higher magnification showing the nature of embrittlement

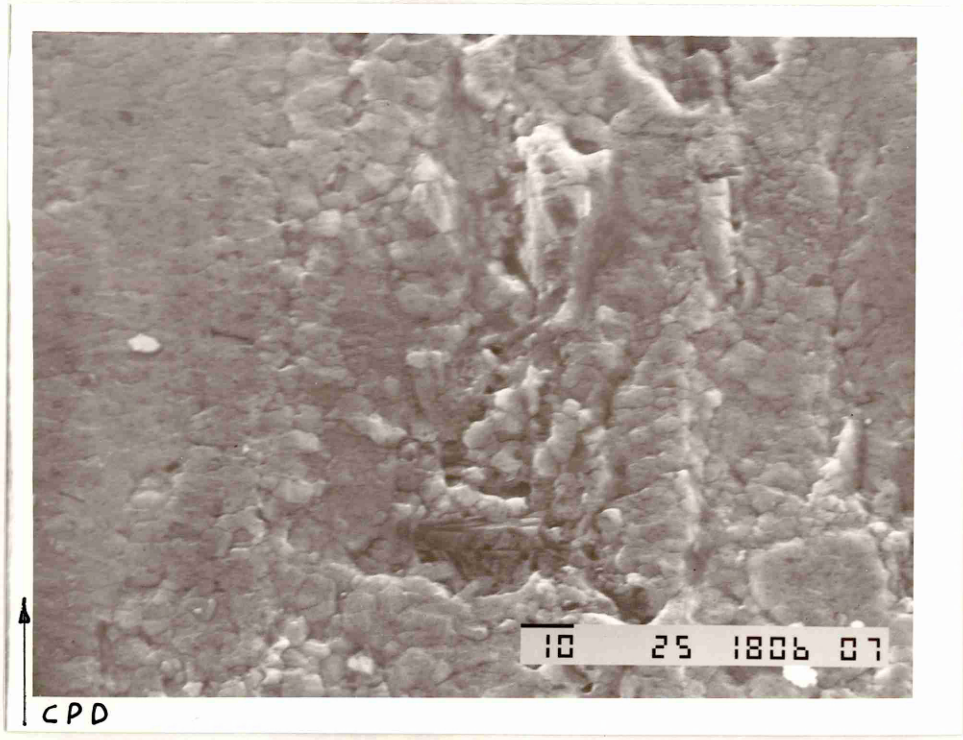

Fig 31 b)

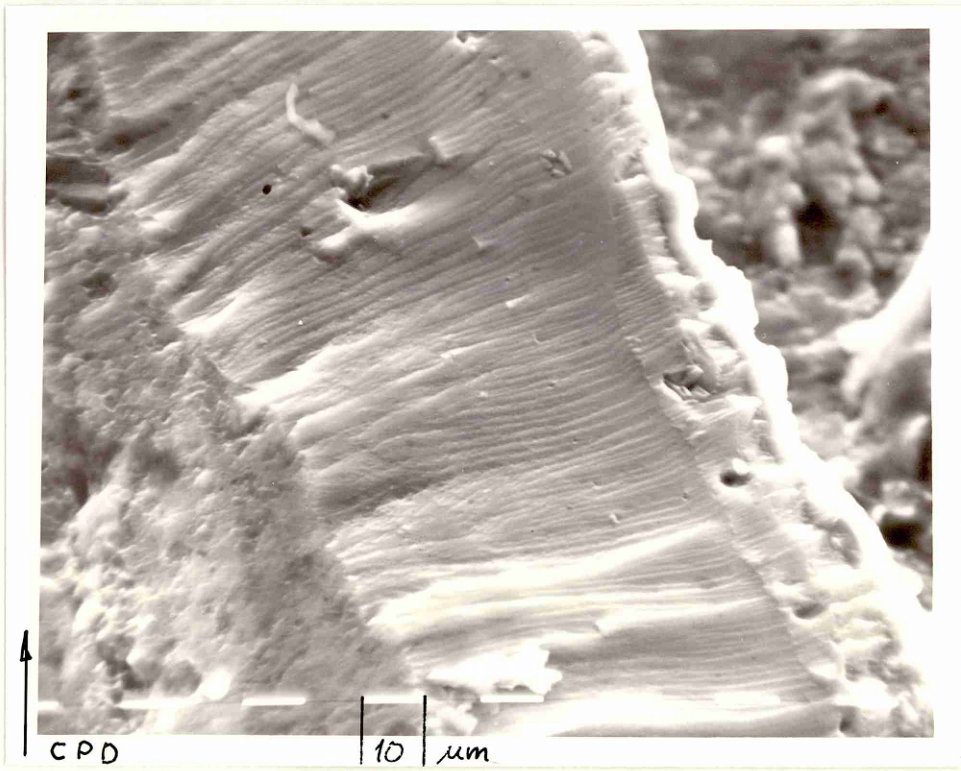

Fig 32 Fatigue striations from specimen fatigued at 25 Hz in lab air, pre-loaded to -8 kN, mean load -0.5 kN ± 0.5 kN